NASA/TM—2012–216004

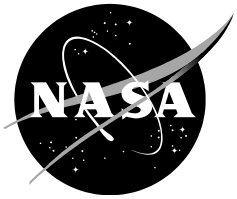

# Wind-Tunnel and Flight-Test Results for the Measurements of Flow Variables at Supersonic Speeds Using Improved Wedge and Conical Probes

*Percy J. Bobbitt and Domenic J. Maglieri*
*Eagle Aeronautics, Inc.*
*Newport News, VA*

*Daniel W. Banks and Michael A. Frederick*
*Dryden Flight Research Center*
*Edwards, CA*

*Aaron W. Fuchs*
*Jacobs Technology, Inc.*
*Hampton, VA*

**December 2012**

# NASA STI Program ... in Profile

Since its founding, NASA has been dedicated to the advancement of aeronautics and space science. The NASA scientific and technical information (STI) program plays a key part in helping NASA maintain this important role.

The NASA STI program operates under the auspices of the Agency Chief Information Officer. It collects, organizes, provides for archiving, and disseminates NASA's STI. The NASA STI program provides access to the NASA Aeronautics and Space Database and its public interface, the NASA Technical Report Server, thus providing one of the largest collections of aeronautical and space science STI in the world. Results are published in both non-NASA channels and by NASA in the NASA STI Report Series, which includes the following report types:

- TECHNICAL PUBLICATION. Reports of completed research or a major significant phase of research that present the results of NASA Programs and include extensive data or theoretical analysis. Includes compilations of significant scientific and technical data and information deemed to be of continuing reference value. NASA counterpart of peer-reviewed formal professional papers but has less stringent limitations on manuscript length and extent of graphic presentations.

- TECHNICAL MEMORANDUM. Scientific and technical findings that are preliminary or of specialized interest, e.g., quick release reports, working papers, and bibliographies that contain minimal annotation. Does not contain extensive analysis.

- CONTRACTOR REPORT. Scientific and technical findings by NASA-sponsored contractors and grantees.

- CONFERENCE PUBLICATION. Collected papers from scientific and technical conferences, symposia, seminars, or other meetings sponsored or co-sponsored by NASA.

- SPECIAL PUBLICATION. Scientific, technical, or historical information from NASA programs, projects, and missions, often concerned with subjects having substantial public interest.

- TECHNICAL TRANSLATION. English-language translations of foreign scientific and technical material pertinent to NASA's mission.

Specialized services also include organizing and publishing research results, distributing specialized research announcements and feeds, providing help desk and personal search support, and enabling data exchange services.

For more information about the NASA STI program, see the following:

- Access the NASA STI program home page at *http://www.sti.nasa.gov*

- E-mail your question via the Internet to help@sti.nasa.gov

- Fax your question to the NASA STI Help Desk at 443-757-5803

- Phone the NASA STI Help Desk at 443-757-5802

- Write to:
  NASA STI Help Desk
  NASA Center for AeroSpace Information
  7115 Standard Drive
  Hanover, MD 21076-1320

NASA/TM—2012–216004

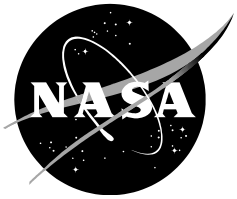

# Wind-Tunnel and Flight-Test Results for the Measurements of Flow Variables at Supersonic Speeds Using Improved Wedge and Conical Probes

*Percy J. Bobbitt and Domenic J. Maglieri*
*Eagle Aeronautics, Inc.*
*Newport News, VA*

*Daniel W. Banks and Michael A. Frederick*
*Dryden Flight Research Center*
*Edwards, CA*

*Aaron W. Fuchs*
*Jacobs Technology, Inc.*
*Hampton, VA*

National Aeronautics and
Space Administration

*Dryden Flight Research Center*
*Edwards, CA 93523-0273*

**December 2012**

Available from:

NASA Center for AeroSpace Information
7115 Standard Drive
Hanover, MD 21076-1320
443-757-5802

# Abstract

The results of supersonic wind-tunnel tests on three probes at nominal Mach numbers of 1.6, 1.8 and 2.0 and flight tests on two of these probes up to a Mach number of 1.9 are described. One probe is an 8° half-angle wedge with two total-pressure measurements and one static. The second, a conical probe, is a cylinder that has a 15°, semi-angle cone tip with one total-pressure orifice at the apex and four static-pressure orifices on the surface of the cone, 90° apart, and about two-thirds of the distance from the cone apex to the base of the cone. The third is a 2° semi-angle cone that has two static ports located 180° apart about 1.5 inches behind the apex of the cone. The latter probe was included since it has been the "probe of choice" for wind-tunnel flow-field pressure measurements (or one similar to it) for the past half-century. The wedge and 15° conical probes used in these tests were designed for flight diagnostic measurements for flight Mach numbers down to 1.35 and 1.15 respectively, and have improved capabilities over earlier probes of similar shape.

The 15° conical probe also has a temperature sensor that is located inside the cylindrical part of the probe that is exposed to free-stream flow through an annulus at the apex of the cone. It enables the determination of free-stream temperature, density, speed of sound, and velocity, in addition to free-stream pressure, Mach number, angle of attack and angle of sideslip. With the time-varying velocity, acceleration can be calculated. Wind-tunnel tests of the two probes were made in NASA Langley Research Center's Unitary Plan Wind Tunnel (UPWT) at Mach numbers of 1.6, 1.8, and 2.0.

Flight tests were carried out at the NASA Dryden Flight Research Center (DFRC) on its F-15B aircraft up to Mach numbers of 1.9. The probes were attached to a fixture, referred to as the Centerline Instrumented Pylon (CLIP), under the fuselage of the aircraft. Problems controlling the velocity of the flow through the conical probe required for accurate temperature measurements are noted, as well as some calibration problems of the miniature pressure sensors that required a re-calculation of the flow variables. Data are presented for angle of attack, pressure and Mach number obtained in the wind tunnel and in flight. In the wind tunnel some transient data were obtained by translating the probes through the shock flow field created by a bump on the wind-tunnel wall.

# Introduction

The accurate measurement of Mach number, pressure and angle of attack at transonic and supersonic speeds is important for many reasons in carrying out flight research, such as accurately defining the instantaneous in-flight conditions of the generating and probing aircraft as well as the generating aircraft's flow field. It could also be important in minimizing focused booms by aiding in the control of the ascent and descent of supersonic-capable aircraft. Changes in altitude and attitude and the resulting changes in free-stream pressure and temperature along with changes in velocity all contribute to Mach number variations. The 15° conical and wedge probes described herein enable one to acquire, and display in real time, Mach number as well as angle of attack. There have been conical probes developed and used before, but the one described herein has additional capability or utility. It makes a temperature measurement, which allows it to determine, in addition to the aforementioned quantities, free-stream static and total temperature, speed of sound, velocity, and acceleration. The wedge probe utilized in the present investigation was similar to the one designed and fabricated in 1992 and described in reference 1. It has about twice the width of the 1992 version, i.e., about one inch, which permits it to make measurements down to Mach numbers of ~1.35. Successful wind-tunnel tests of the original wedge probe have already been made (ref. 1), however, the wedge probe has never been flight-tested. The accuracy of the conical and wedge probe measurements is enabled, in part, by taking advantage of the exact analyses of conical flow carried out as far back as 1933 (refs. 2 to 8); and the wedge probe to those in references 4, 5, and 8.

Another feature of significance regarding the conical and wedge probes is their ability to acquire data in a near instantaneous fashion. This is due to the instantaneous response of the pressure sensors to a change in pressure and the close proximity of these pressure gages to the pressure ports. Thus, if these probes are on the front end of a probing aircraft, there is no restriction on how fast the probing aircraft can traverse the flow field of the supersonic generating aircraft. Similarly, in a traverse of the flow field of a generating model in a supersonic wind tunnel there is no reason to stop and go at each point when a measurement is made. Also, in flight, the measured flow field signatures are less likely to be altered by changes in the generating airplane's altitude, Mach number and separation distance. In the wind tunnel, the required traverses can be accomplished in much less time.

Wind tunnel tests of the two probes were made in NASA Langley Research Center's Unitary Plan Wind Tunnel (UPWT) at Mach numbers of 1.6, 1.8 and 2.0. Measurements were made of the basic wind-tunnel flow quantities and compared to those measured by the wind-tunnel system, as well as the variations of the flow quantities across the flow field generated by a 5-inch bump on the wind-tunnel wall.

Flight tests were conducted at NASA's Dryden Flight Research Center in March and April of 2011. They were carried out with the probes attached to a fixture on the underside of the fuselage of a NASA F-15B aircraft. Data from both the wind-tunnel and flight tests will be presented, and described later in this paper.

# Nomenclature

| | |
|---|---|
| $\alpha$ | angle of attack |
| $\beta$ | angle of sideslip |
| $\gamma$ | ratio of specific heat |
| h | distance from centerline of wing or body |
| H | total pressure |
| *l* | length of wing or body |
| M | Mach number |
| P | pressure |
| $\Delta p$ | difference between local and free-stream static pressure |
| q | dynamic pressure |
| R | unit Reynolds number |
| $\theta_V$, $\theta_H$ | flow angle in vertical and horizontal planes |
| T | temperature |
| V | velocity |
| x | longitudinal distance |
| y | lateral distance |
| z | vertical distance |

**Subscripts**

| | |
|---|---|
| c | value on cone |
| i | inside the conical probe |
| meas, measured | indicates temperature measured by temperature sensor in conical probe or pressures by pressure gages |
| s | stagnation |
| t or tot | total or stagnation value |
| $\infty$, inf | static value in free stream or that just ahead of probes in flight test |
| 1 | static value inside cone |
| 2 | total value inside cone |

# Background

The use of probes to measure various free-stream flow quantities is as old as flight itself. Pitot tubes for the measurement of pressures that, in turn, yield flow velocity are the most common and well known. Diagnostic probes specifically tailored for supersonic measurements probably got started in the late 1930s, when the capability to produce supersonic flows using blow-down tunnels originated. Reference 9, published in 1949, details a number of devices for measuring pressure, Mach number, and density. Included is the use of wedges, in different arrangements, to measure flow angle, pressure and Mach number. Figure 1 shows the arrangement of pressure taps on both sides of a wedge and equally spaced on the surface of a cone, which enables flow angle calculations using the appropriate equations.

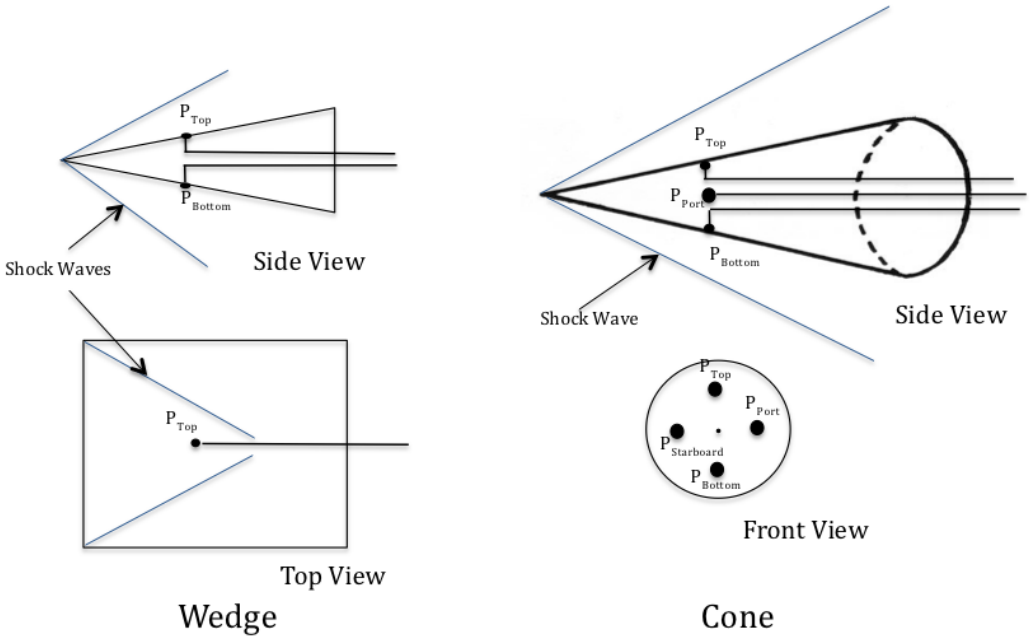


Figure 1. Wedge and cone instruments for the measurement of the flow direction.

Figure 2, from reference 10, shows a wedge probe used at the NASA Lewis Research Center (now John Glenn Research Center). It has two total-pressure measurements, behind the leading-edge shock and two static-pressure taps. The wedge angle is 20° and it is 6 inches in width. With its size, it evidently was used for free-stream measurements rather than detailed diagnostics. Also due to the wedge angle of 20°, it must have been limited to Mach numbers above 1.84.

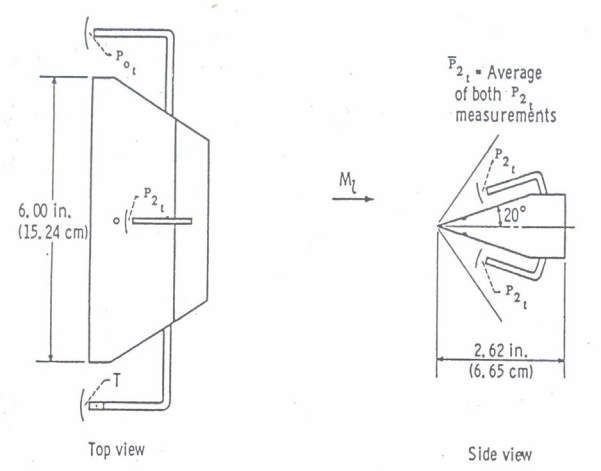


Figure 2. Details of large wedge probe design (from ref. 10).

Reference 11 by Gorlin and Slezinger is a compilation of information concerning wind tunnels and their instrumentation. It discusses wedge, conical, and pyramid probes, but most are single-purpose devices that measure Mach number (see fig. 3a) or flow direction or density, etc. It is a valuable resource because of its scope (592 pages) and other relevant papers that it references, such as reference 12.

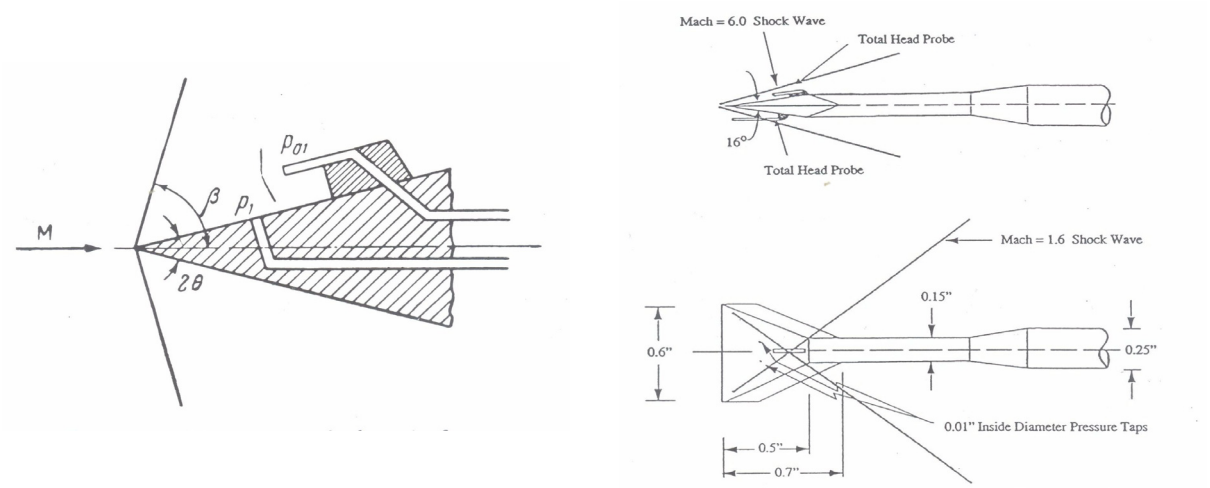


a. Wedge-shaped obstacle for measuring Mach number.

b. Wedge probe showing relationship of corner and leading-edge shocks to pressure sensors (from ref. 1).

Figure 3. Small wedge probe designs.

The wedge probe described in the Introduction (see ref. 1) and shown in figure 3b, is much smaller, 0.6 inches in width, and all of the three pressure measurements are made within 0.3 inches of the leading edge, enabling very high resolution. The mathematics used to determine the free-stream flow quantities are exact, based on the Euler equations (see Appendix A).

Conical probes with a half-apex angle of 15° have been used by NASA researchers in several flow-diagnostic research projects and documented in references 13 and 14. The geometry of the probe used in reference 13 is shown in figure 4. With a diameter of 0.1875 inches, the pressure orifices on the cone forebody are all within 0.2 inches of each other and the resolution is outstanding. The equations used to determine Mach number and flow angle from the measured pressures on the forebody (15° cone) are given in the paper and repeated in Appendix B. They were also used in the present investigation.

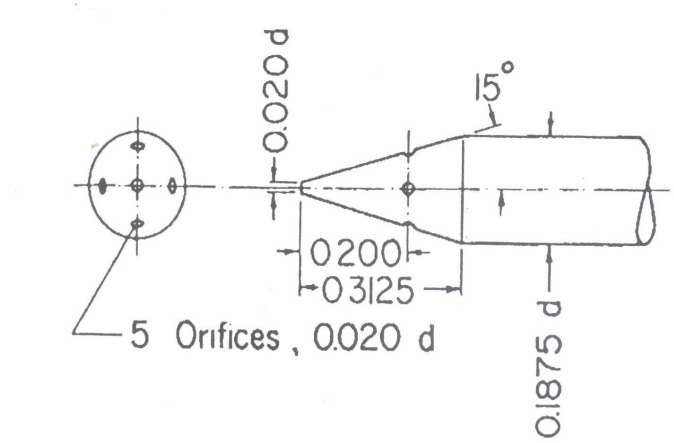


Figure 4. Details of conical probe, all dimensions are in inches (from ref. 13).

The cone geometry of the probe used in reference 14 is shown in figure 5 with its diameter of 0.189 inches (0.48 cm). Thus, it was essentially the same size as that of reference 13 and had the same resolution.

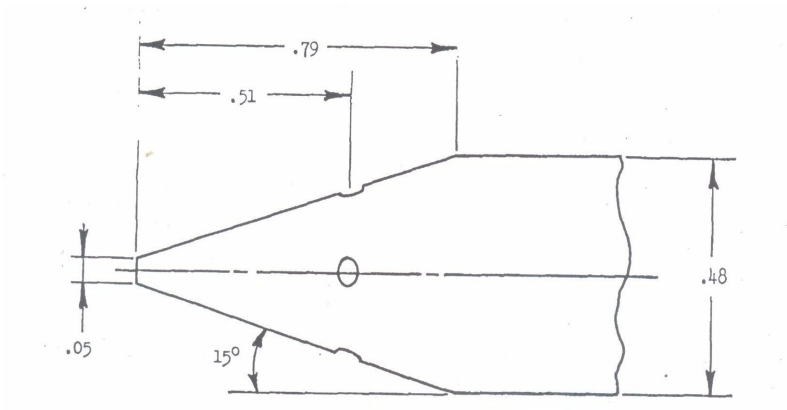


Figure 5. Sketch of conical probe. All dimensions are in centimeters unless otherwise noted (from ref. 14).

In addition to the wedge and conical probes, a 2° semi-apex angle cone was also used in the present investigation. It has been the "probe of choice" for wind-tunnel pressure measurements since the early 1960s. Due to the location of the static pressure ports and the length of the probe (see fig. 6a) there are some intrinsic error sources.

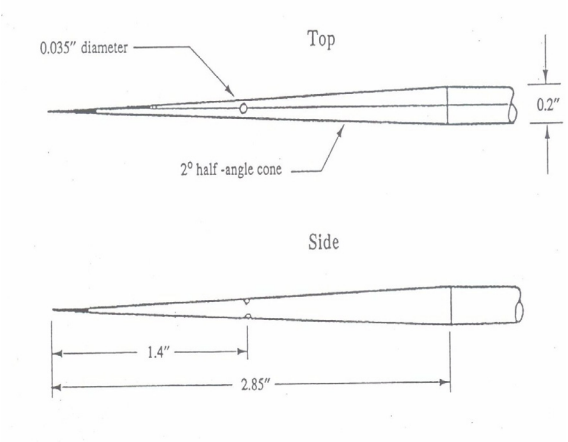


a. Geometry of conical pressure probe with 2° half-angle. Pressure orifices on top and bottom.

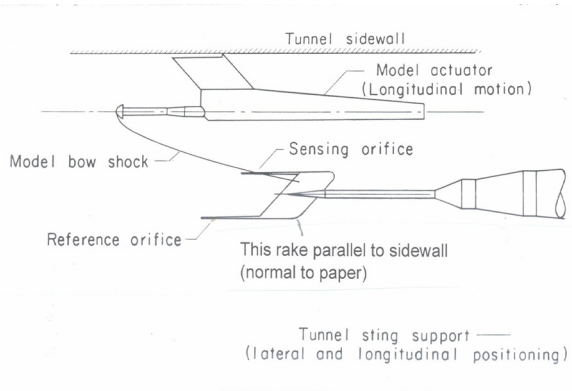


b. Sketch showing sidewall-mounted model and rake with pressure probes.

Figure 6. Small angle cone for free-stream pressure measurement.

One possible error source is the assumption that the measured pressure on the cone is the same as the free-stream static pressure. Plots of $(P_c - P_\infty) / (q_\infty)$ in reference 7, e.g., indicate a value of 0.008 for this parameter at a Mach number of 2.0 for a $2^0$ semi-vertex-angle cone. With

$$q_\infty = \frac{\gamma}{2} M_\infty^2 P_\infty$$

$(P_c - P_\infty) / (q_\infty)$ becomes

$$\frac{P_c - P_\infty}{2\gamma P_\infty} = 0.008$$

or

$$P_c = (1 + 0.0224)\, P_\infty = 1.0224\, P_\infty$$

So, there is an error of ~2 percent at this Mach number just due to the fact that the pressures are measured at the surface of a 2° cone.

If one assumes a total pressure of 940 psf and a nominal static pressure of 120 psf in the equation for this parameter at a Mach number in terms of the ratio of total to static pressure, given below:

$$M_\infty = \sqrt{5\left[\left(\frac{H}{P_\infty}\right)^{2/7} - 1\right]}$$

Then one can determine the error in Mach number corresponding to the error in static pressure. For the same Mach number and the 2.24 percent error in $P_\infty$ measurement it is 0.6 percent. Use of the plot in reference 7 for the Mach number on cones versus cone angle indicates, for a free-stream Mach number of 2.0, the Mach number on the cone is 1.98. For lower total pressures the errors will be higher. It should be noted that this probe is not nominally used for Mach number measurements. Also, for conical probes with a 1° semi-apex angle, such as that used in references 15 and 16, and probably in reference 17 as well, the errors would be roughly one-half of those calculated above for a 2° semi-apex angle cone.

In most of the tests using the 2° semi-apex angle cone probe, a second 2° cone probe was used, as seen in figure 6b, to measure the static pressure in the free stream (see refs. 18 through 21). This measurement was then subtracted from that of the probe in the disturbed flow field to yield a more accurate measurement of the incremental pressure provided by the test model. It should be noted, however, that this increment is also processed by the shock system of the 2° cone.

Another error occurs when flow-field shocks intersect the cone in the vicinity of the pressure taps. If the probe has four taps and they are aligned vertically, and the probe is below the model, the bottom tap will see the shock before those on the side or top. To reduce this error, some experimenters have aligned the pressure taps with the expected incoming shock (see refs. 20 and 22).

In 1977 and 1959, papers by Carlson and Mack (refs. 20 and 23) and in 1979 Mack and Darden (ref. 21) reported using a 2° semi-angle cone probe with pressure taps on the top and bottom as in figure 6. However, it was oriented with the line through the two pressure taps normal to the plane of the model and the probe, i.e. the holes are in the horizontal plane versus the vertical. Thus, the two pressure taps sensed the incoming shocks at the same time. This was an important characteristic, particularly for small models, in the selection of the 1° and 2° semi-angle cones in the early days of sonic boom experimentation.

There is also a very thin boundary layer on the cone which, when it interacts with the shock, allows the pressure orifices to feel the shock pressure rise before it actually reaches the orifice as well as after the shock has gone beyond the orifice. Figure 7, from reference 22, shows the shock- smearing produced by the probe for a 60° delta wing. This wing had a 0.5-inch chord and was at 10° angle of attack. Clearly, the larger the length of the model relative to the length of the probe the less effect the smearing will have. Note that there is even more smearing on the boundary layer by-pass plate measurement which is all due to shock boundary-layer interaction. See reference 10 for additional discussion of the shock smearing phenomena. It should be noted that prior to 1960 the boundary-layer bypass plate was the preferred instrument for measuring flow-field pressure (see ref. 23).

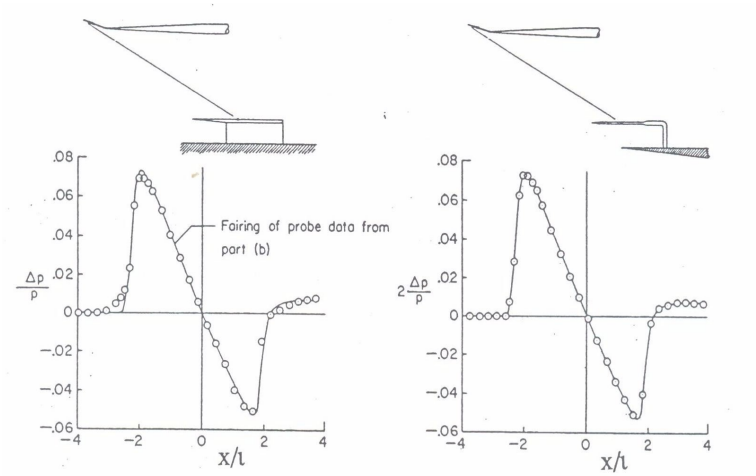


Figure 7. Comparison of pressure measurements made with a reflection plate and with a probe (from ref. 22). $60^o$ delta wing; a = $10^o$; h/*l* = 16; M = 2.01.

## Description of New Wedge and Conical Probes

The wedge probe used in the current measurements is twice as wide as that of reference 1 (see fig. 8) in order to allow measurements down to a Mach number of 1.35. With this width it keeps the shock from the corners of the wedge from passing in front of the static ports on the surface in the middle of the wedge. The probe of reference 1 was configured for Mach numbers of 1.6 and above. The distance between the total pressure tube on the bottom side of the wedge and the total pressure tube on the top side, i.e., 0.25 inches (see fig. 8), is the distance that an incoming shock from a wind-tunnel model or another airplane would be resolved. This distance could be reduced some by moving the top-side total pressure tube forward, e.g., to where it is aligned with, or ahead of, the static pressure ports. Obviously, it cannot be moved so far forward that the shock off its front end impacts the wedge surface ahead of the static pressure ports. Other arrangements of the static pressure ports and the top side total pressure tube are possible. For full-scale in-flight probing the incoming free-stream flow, the distance between the static ports and total pressure tubes is of no consequence.

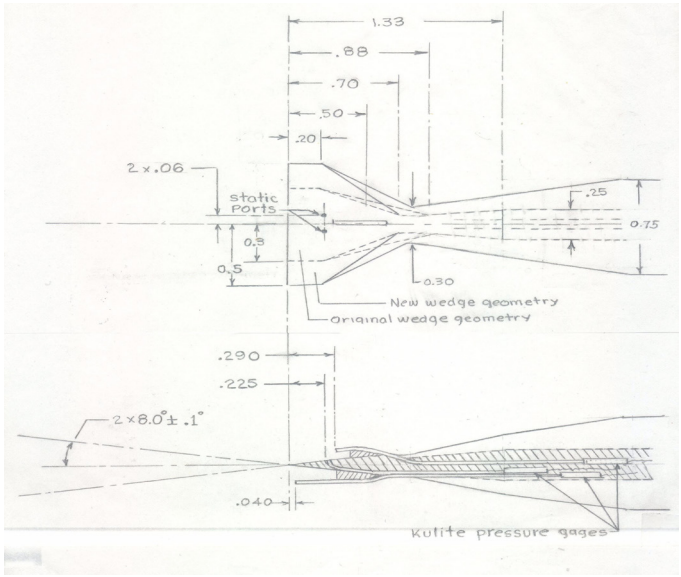


Figure 8. Details of wedge probe design.

The pressure measurements are made using cryogenic ultra-miniature pressure gages that are stated to be capable of temperature compensated measurements from -320 °F to 100 °F (-196 °C to 38 °C) with infinitesimal resolution. The operating range can extend up to +250 °F (121 °C). Three miniature pressure transducers were installed in the wedge probe; one to measure static pressure and two that measure total pressure (at different places). These are absolute pressure gages of 5 psia and 10 psia, respectively. They are purported to be linear up to two times rated pressure and the bursting pressure is three times rated pressure. The gages are located in the probe body just downstream of the wedge itself. Thus, there is a minimal time delay from the actual sensing of pressure at the orifices to the sensing by the miniature pressure transducers. This is a great advantage in recording a transient event such as the varying pressures measured by one supersonic aircraft penetrating the flow field of another or an airplane's acceleration.

The conical probe used in this investigation is shown in the schematic of figure 9 and is intended for flight measurements down to Mach numbers of 1.15. In addition to utilizing the same type of pressure gages used in the wedge probe, it includes a temperature sensor and one additional pressure sensor that is used to correct the temperature measured inside the probe to the free-stream stagnation temperature. Using this additional measurement free-stream density, temperature, speed of sound, and velocity may be determined as well as pressure, Mach number and flow angle (angle of attack and angle of sideslip). Measurements made using the conical probe are used in the equations of Appendix B to determine free-stream quantities. With the inclusion of the temperature sensor and the fact that the conical probe was to be used primarily for flight measurements, the diameter was set at 0.75 inches. Thus, in the wind-tunnel measurements, shock jumps and steep gradients are smeared more than those for the 0.1875-inch diameter conical probes described earlier.

The conical probe tested in the 4-foot Unitary Plan Wind Tunnel had its total-pressure orifice in a cup just downstream of the conical part of the probe (see fig. 9). This was done to facilitate flow through the gage from the apex orifice. Obviously, to make the temperature measurement in a changing environment there must be flow through the gage. However, data for the response of the temperature sensor to a changing environment are available only for water. Thus, the amount of air flow through the gage to measure a changing external temperature was set by the need to maintain a low flow velocity in the vicinity of the total-pressure gage in the cup (see fig. 9). The desired velocity was 15 to 20 ft/sec, which is about 3 or 4 times the required rate in water. It was thought, based on area and mass flow considerations, that a 0.06-inch diameter apex hole and four 0.125-inch vent holes at the back end would yield the desired velocity.

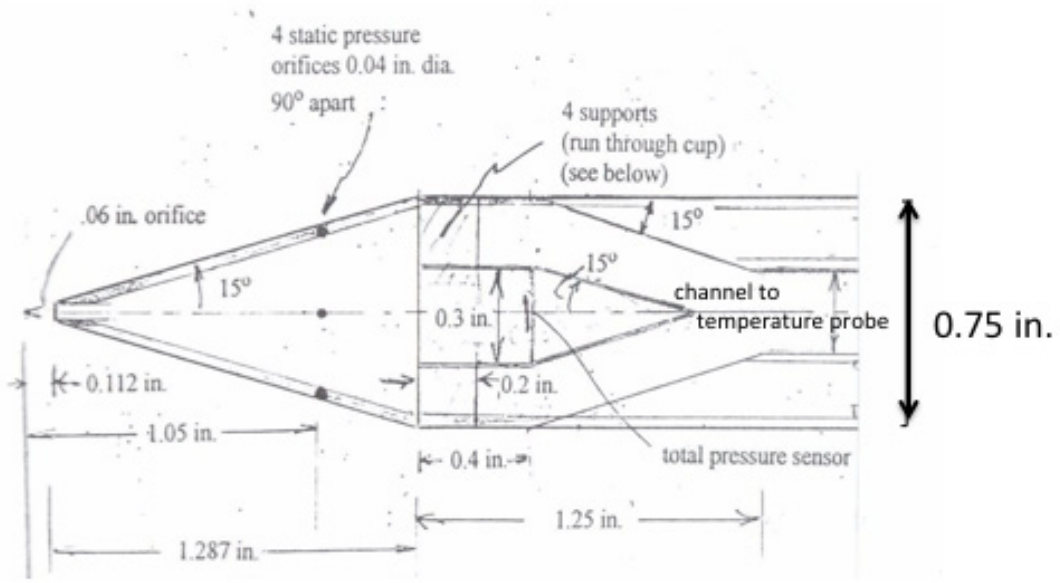


Figure 9. Details of conical probe design.

The first test in the Unitary Plan Wind Tunnel (UPWT) did not shed much light on the flow rate through the conical probe since the back end was not fully sealed and the flow through the inside of the cone was clearly much larger than expected. Subsequently, in the second test, additional leaks were found and eventually sealed to lend added concern about the "flow-through" problem.

The flow velocity in the channel containing the temperature probe (see fig. 9) is measured using a pressure gage (and orifice) just ahead of the temperature probe, and the total pressure, as noted, in the cup. The latter orifice was located beneath a cruciform divider that inhibits any induced flow (see fig. 9).

In the second, and definitive, wind-tunnel test series it became clear that total pressure in the cup did not give an accurate measurement based on the total pressure measurements made by the wedge probe. In many cases the total pressure measured in the cup was smaller than the static pressure measured in the channel. It was also clear that one reason for this problem was the inability to achieve a flow velocity inside the gage as low as 15 ft/sec by varying the vent-hole sizes in the back end. Velocities of this magnitude, or lower, enable the stagnation and the channel pressure to be within 0.1 percent or less of each other, as can be seen in figure 10, and the measured stagnation pressure will be trivially different from the exact stagnation value. Figure 10 shows the variation of the channel velocity with the ratio of the total pressure ($H_t$) to channel pressure ($P_i$) for an altitude of 40,000 ft and a Mach number of 2.0 at standard atmospheric conditions. For a ratio of $H_t$ and $P_i$ of 1.001 (or 0.1 percent) the velocity is 16 ft/sec.

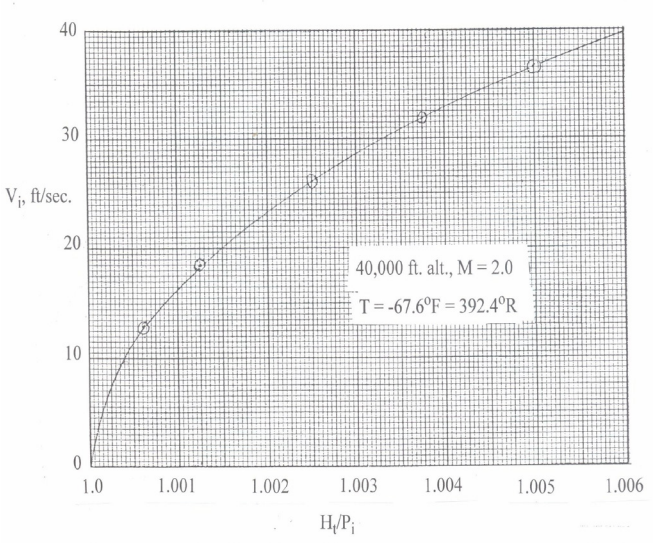


Figure 10. Variation of velocity in the channel ahead of the temperature probe versus the ratio of total pressure behind the shock to the pressure measured in the channel at typical flight conditions.

As a result of the wind-tunnel tests, it was decided to move the total pressure orifice to the apex of the cone. Thus, there is an annulus around the total pressure tube at the apex of the cone as seen in the sketch and photograph of figure 11. The apex hole is twice the diameter of the total pressure tube and an adjustable sleeve, with vent holes of various sizes, is at the back of the probe. Four 0.03125-inch vent holes were used. This vent-hole sizing was based on tests made during the wind-tunnel tests. With this arrangement the total-pressure measurement will be accurate and the temperature sensor, with the higher flow-through velocity, will be able to respond more quickly to changes in free-stream temperature than the original design. The need to have a low flow velocity, in order to make an accurate total pressure measurement in the cup, is no longer required.

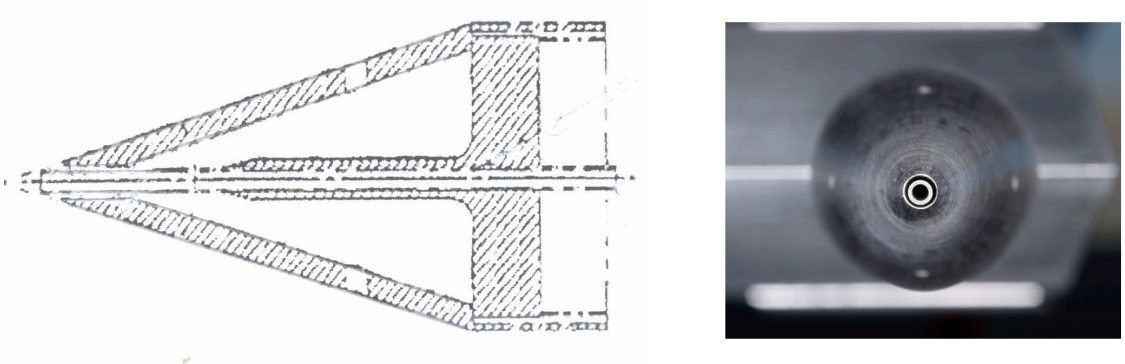

(a) Sketch of cross section of cone. (b) Photograph of apex of cone.

Figure 11. Sketch and photograph showing total-pressure tube at apex of cone and annulus around it.

It should be noted that due to the problems with the total pressure measured in the cup, the stagnation pressure measured by the wedge probe was used (since it was located nearby) for the wind-tunnel data reduction for the conical probe.

With the movement of the total-pressure sensor to the apex of the cone, as seen in figure 11, the conical probe used in the flight tests has the appearance shown in figure 12. The modified nose cone, as well as the other components, are labeled in this figure. The sleeve used to change vent-hole size is item 13 in this figure.

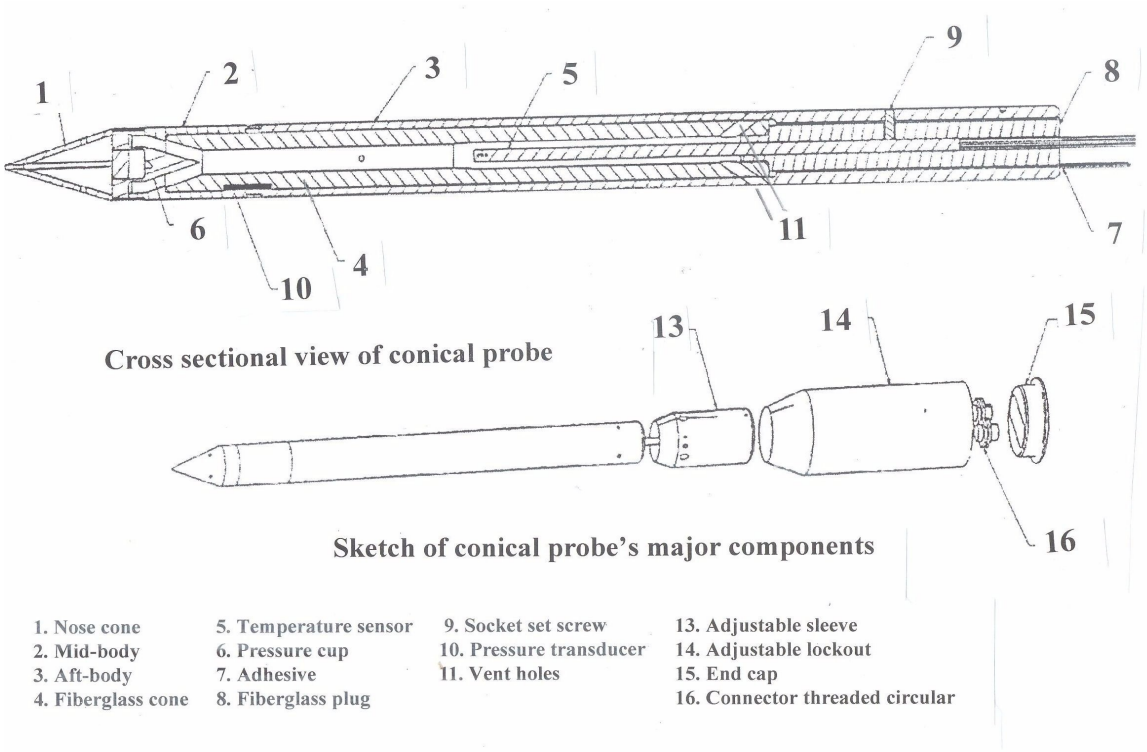


Figure 12. Details of conical probe design.

## Test Facility

The test results detailed in the next section were carried out in the Langley Unitary Plan Wind Tunnel (ref. 24). It is a closed-circuit pressure tunnel with two 4 x 4 x 7 feet (1.22 x 1.22 x 2.13 m) test sections. An exterior view of the facility is shown in figure 13, a schematic drawing of the arrangement of the major elements is shown in figure 14, and a detailed planform of the wind-tunnel circuit arrangement is shown in figure 15. The major elements of the facility are the 100,000 hp (74.6 MW) drive system, a dry air supply and evacuating system, a cooling system, and the interconnecting ducting to produce the proper airflow through either of the two test sections.

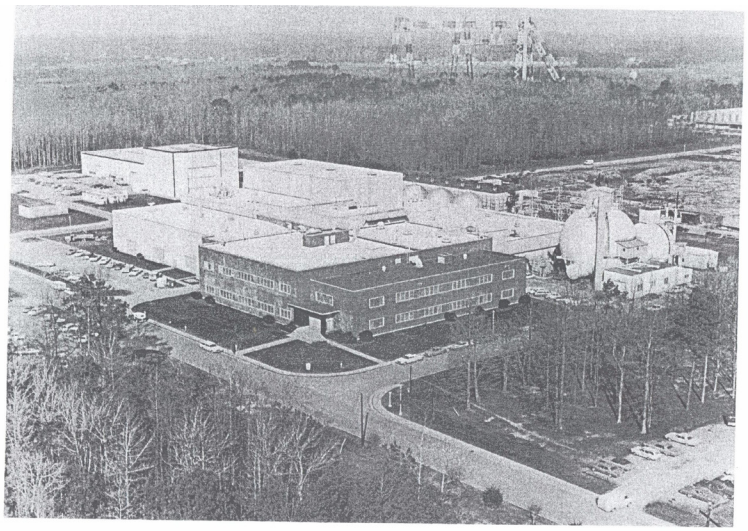

Figure 13. Photograph of the Langley Unitary Plan Wind Tunnel (from ref. 24).

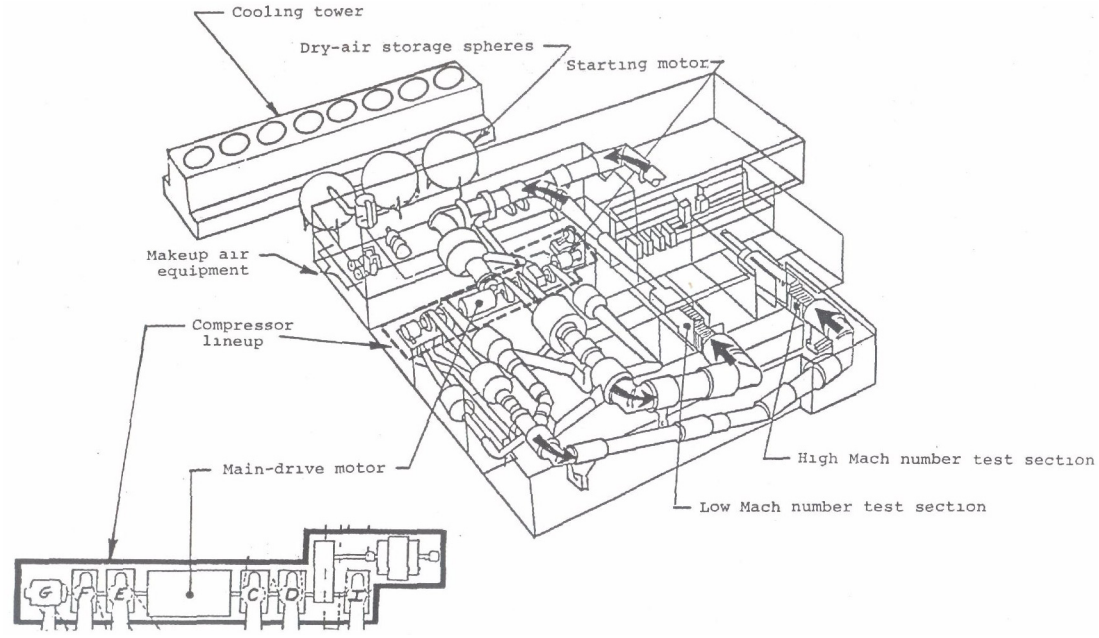


Figure 14. Schematic drawing of the Langley Unitary Plan Wind Tunnel (from ref. 24).

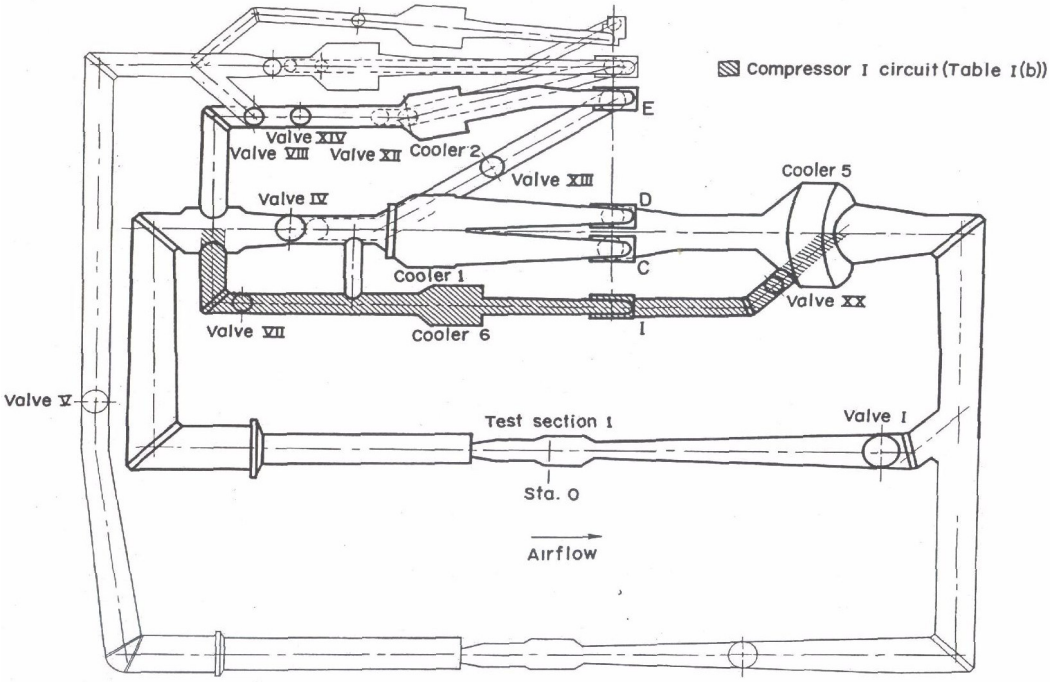


Figure 15. Low Mach number circuit (from ref. 24).

The low Mach number circuit shown in figures 14 and 15 (Test Section 1) was used for the present tests. These tests were conducted at nominal Mach numbers of 1.6, 1.8, and 2.0. Most tests were run at free-stream stagnation pressures of approximately 40 to 45 percent of an atmosphere.

## Shock Generator

In order to determine the ability of the probes to measure transient, non-uniform flows, a side wall disturbance bump was installed. This disturbance bump has the geometry shown in figure 16 and produces a shock across the test section of ~0.32 psia at Mach number of 2.0. It has a circular arc surface geometry, a chord of 5 inches and a maximum thickness of 0.5 inches. Before the second wind-tunnel entry a "secondary shock" bump was added in hopes of a generating a shock of about one-tenth that of the main shock. Its geometry is shown by the shaded area in figure 16. However, the boundary layer on the test section wall is about 4 inches thick and the disturbance caused by the secondary bump was smeared out. However, a small increase in pressure was detected by the wedge probe, as seen in a later figure.

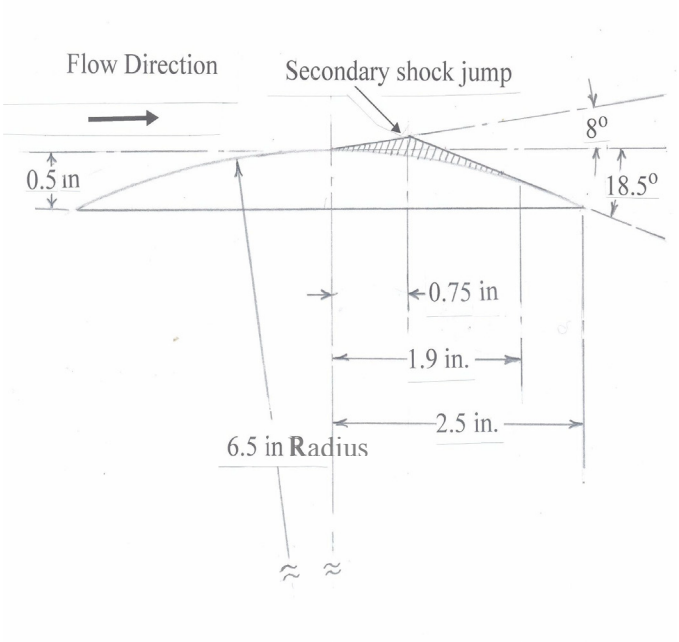


Figure 16. Sketch of wind-tunnel wall disturbance bump design.

## Probe Holder

A probe holder was designed that held the three probes such that the shocks off the apex of each probe did not interfere with an adjacent probe. A photograph of the probe holder with the probes installed is shown in figure 17. A view of the holder in the vertical position, along with the disturbance bump on the sidewall, is presented in figure 18.

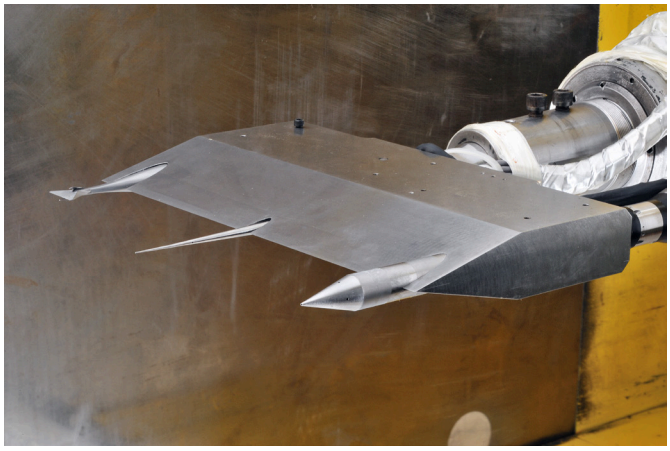

Figure 17. Photograph of three-probe sting arrangement in UPWT.

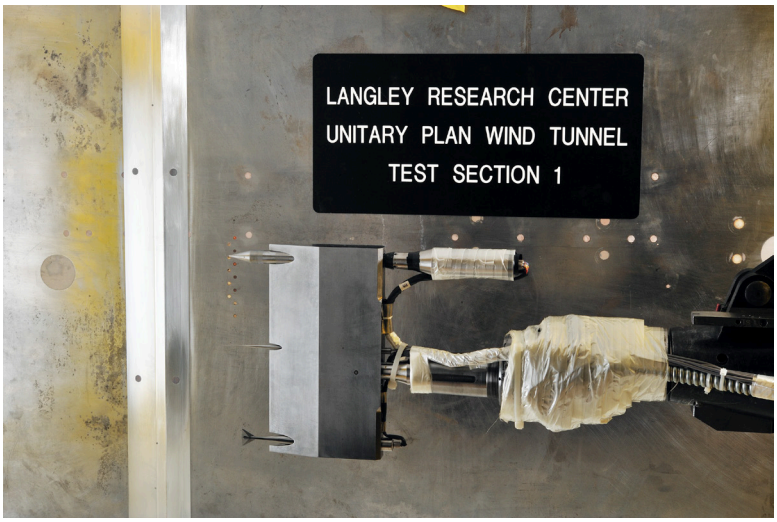


Figure 18. Photograph of probe alignment for wall disturbance bump shocks in UPWT.

The chord of the probe holder was limited by the fact that vent holes on the back end of the conical probe could not be blocked. The apex of the various probes are not lined up so that each probe senses the bow-shock off the shock generator (wall disturbance bump) at a different time as the probes were moved longitudinally through its flow field.

## Wind-Tunnel Flow Quality

The wind-tunnel measurement system for a sting-mounted model includes the geometric angle of attack, static and total pressures, and Mach number. As with any supersonic wind tunnel, there are non-uniformities in all these quantities with the smallest, hopefully, in the region where models are mounted. These gradients are of particular concern in the present tests because the three probes are located about 5.25 inches apart. As such, measurements of flow angle, Mach number, and pressure can be different due to their different locations. There are lateral, vertical, and longitudinal gradients of flow angle and Mach number so that when the static measurements of these quantities are made, with the probes aligned in the lateral direction, they can measure differently due to the lateral gradients. When they are aligned vertically, as they are for the longitudinal transverse, they are subject to vertical and longitudinal non-uniformities.

The rest of this section discusses the details of the flow-field non-uniformities and how they might affect the measurements of the probes.

Reference 24 by Jackson, et al., contains plots of the aforementioned non-uniformities for both test sections one and two. The former is of concern here. Figure 19 shows the longitudinal and lateral variations of Mach number for nominal Mach numbers of 1.769 and 2.16. In the case of the former, data are given for four Reynolds numbers and two vertical heights, and the latter data are presented for two vertical heights and three longitudinal locations. The present tests were conducted at a Reynolds number of ~ $1.5 \times 10^6$ per foot and the 48-inch longitudinal location (square symbols) is the closest to where the probes were located during the static tests.

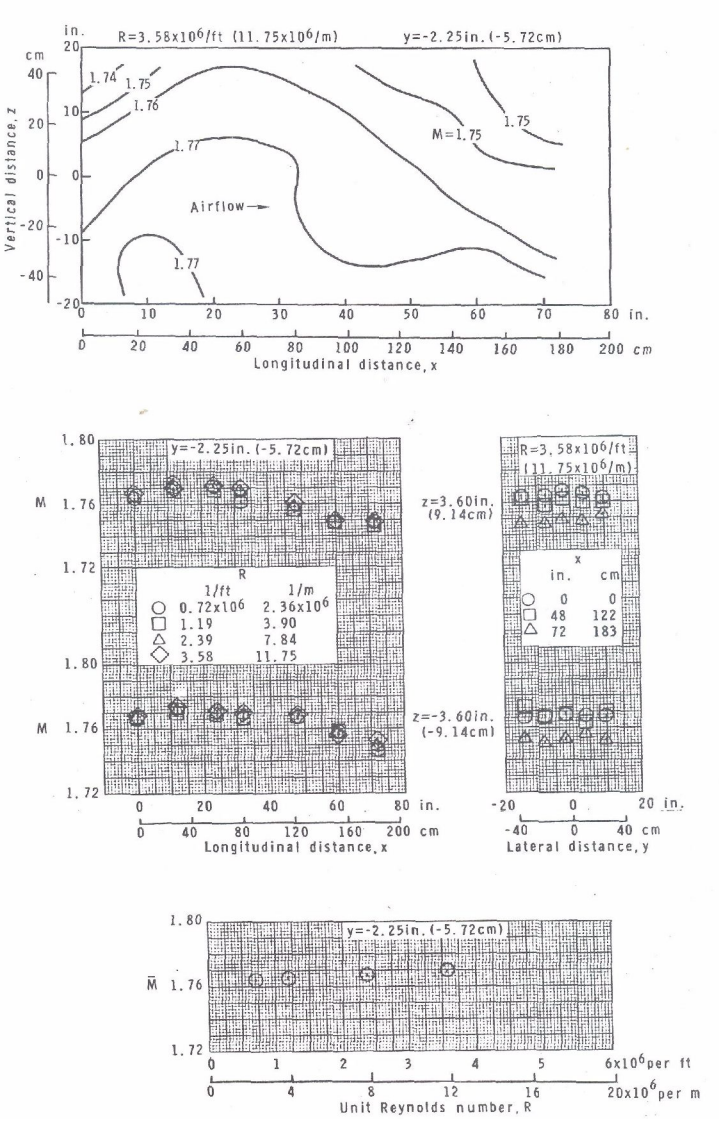


(a) M = 1.769

Figure 19. Mach number distributions in the Unitary Plan Wind Tunnel for two nominal Mach numbers (from ref. 24).

At a nominal Mach number of 1.769 (see fig. 19a) and z = 3.6 inches, the longitudinal distribution of measured Mach numbers from an x of ~ 30 inches to 60 inches yields a gradient of ~ 0.00055 per inch. At a z of -3.6 inches, the uniformity is better with the Mach number at an x = 48 inches equal to 1.766 to 1.769 depending on Reynolds number. Laterally, the variations in Mach number from the nominal at x = 48 inches are roughly +0.004 and -0.006 from the y = 0 values. However, the Mach number level at a z of 3.60 inches is about 0.01 below the nominal.

For a Mach number of 2.16 (see fig. 19b) there are larger variations in Mach number than at a Mach number of 1.769. Note that at a Reynolds number of 1.5 x $10^6$ the longitudinal data of interest are halfway between the square and triangle symbols. Longitudinal distributions of Mach number at z = 3.6 inches show good agreement of the measured Mach number with the nominal up to an x of ~ 48 inches. Beyond this point, the measured Mach numbers fall below the nominal Mach number

of 2.16. At a z of -3.6 inches the trend is opposite and at the 30 and 48 inches points the measured values are quite a bit higher than the nominal.

The lateral variations for a Mach number of 2.16 in figure 19b show similar effects at the two vertical heights, i.e., for a z of 3.6 inches the agreement is pretty good for x values of 0 and 48, but not beyond, and at a z of -3.6 inches the measured values at x = 48 inches and 72 inches are generally higher than the nominal.

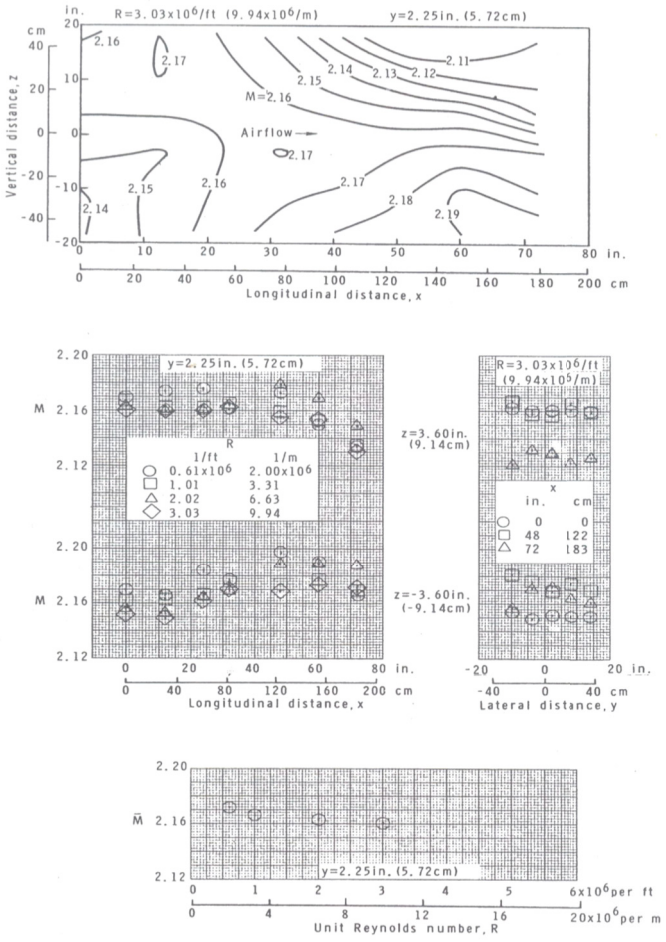


(b) M = 2.160

Figure 19. Concluded.

Variations of flow angle with lateral and longitudinal distances are given for three Mach numbers, 1.57, 1.77, and 1.97, in figure 20. Of primary interest here are the lateral variations of $\theta_V$ (flow angle in vertical planes). Data are given at two vertical heights and at three longitudinal locations. At a Mach number of 1.57 and an x of 50 inches, and a z of +3.6 inches (see fig. 20a) there appears to be a gradient between plus and minus 7 inches of about 0.008°/inch or as much as 0.08° for the 10 inches separating the conical and wedge probes. At z = -3.6 inches at this same station, there is a larger gradient of 0.021°/inch or 0.21° for the 10 inches separating the wedge and conical probes. On average, then, one would expect a 0.15° difference between the two probes (assuming the probes are located at

x = 50 inches) with the higher value at the conical probe. Almost the opposite is seen at a Mach number of 1.77 at the x = 50 inches station (see fig. 20b).

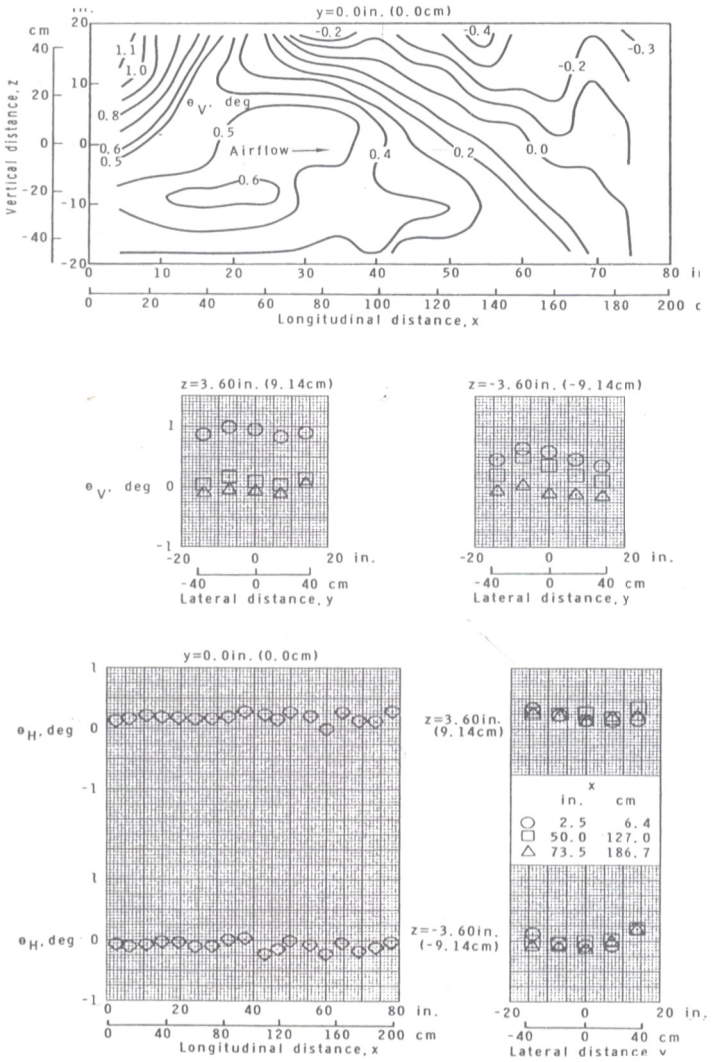


(a) M = 1.57; R = 1.62 x $10^6$ per ft (5.31 x $10^6$ per m).

Figure 20. Flow-angle calibration for test section 1 (from ref. 24).

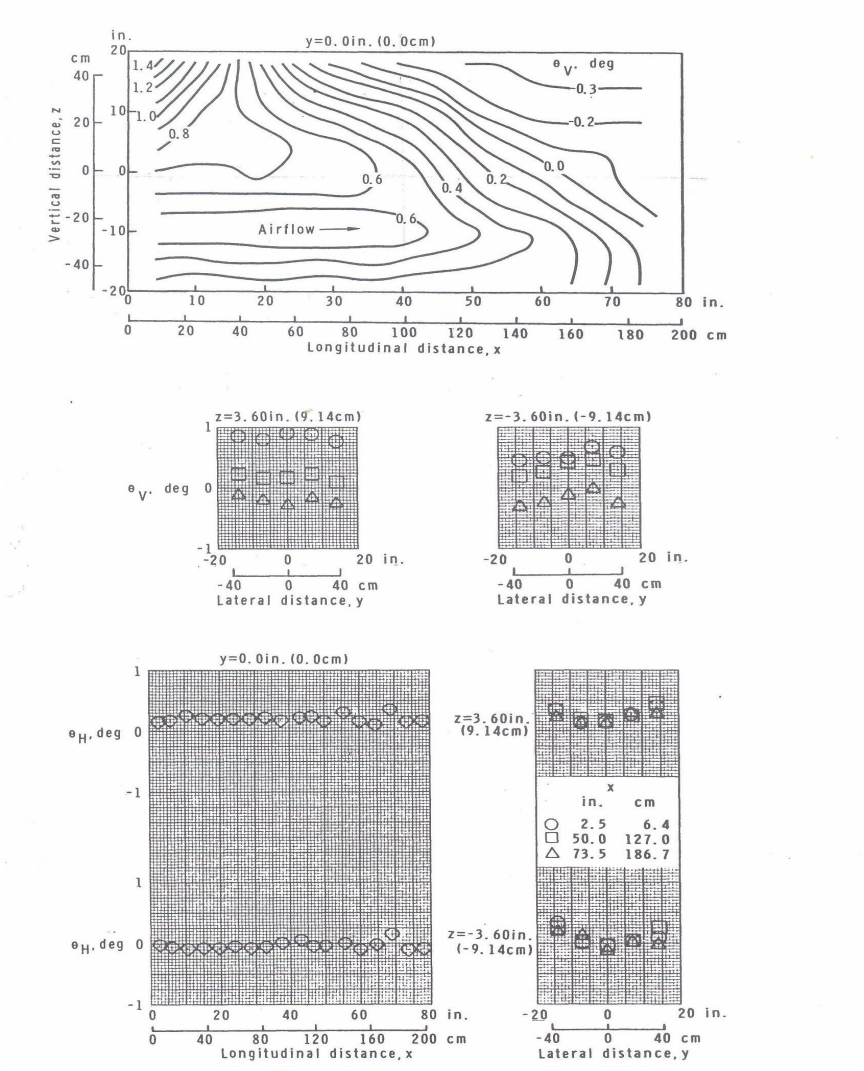


(b) M = 1.77; R = 1.51 x $10^6$ per ft (4.95 x $10^6$ per m).

Figure 20. Continued.

The $\theta_V$ plots for a Mach number of 1.97 (see fig. 20c) show the gradients spanwise are small for all three x locations, and at x = 50 inches the $\theta_V$ is around 0.5°. Thus, you would expect both probes to read about the same, i.e., 0.5° displaced from the wind-tunnel value.

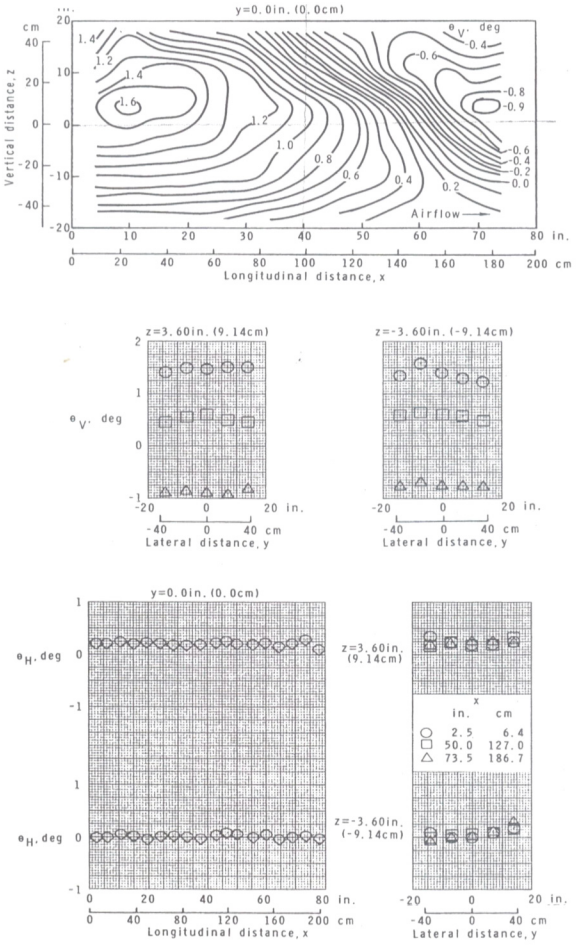


(c) M = 1.97; R = 1.63 x $10^6$ per ft (5.35 x $10^6$ per m).

Figure 20. Concluded.

## Flight Tests

Flight tests of the probes were made at NASA's Dryden Flight Research Center during the months of March and April 2011. The probes were installed on the bottom side of the Centerline Instrumented Pylon, or CLIP, attachment (see fig. 21) installed on NASA's F-15B testbed airplane. The probes were mounted on the CLIP to prove the structural integrity of the probes and to check out the measurement system and the data reduction programs. Figures 21a and 21b, taken from the air, show the entire airplane and a close-up of the CLIP installation, respectively. Figure 21c gives a better idea of the location of the probes relative to the leading edge of the CLIP. The longitudinal location of the front ends of the probes are not the same, with the wedge probe being forward of the conical probe by ~ 1.0 inch (see fig. 22). Note that in regards to the probe flight measurements free stream refers to the immediate upstream conditions with respect to the probes and not true aircraft free-stream values.

At free-stream Mach numbers near 1.6, the shock off the leading edge of the CLIP is in close proximity to the sensor heads and with the wedge probe's more forward location it will be closest to the shock. Consequently, as Mach number increases the shock off the sides of the CLIP will pass over the

wedge probe first. Conversely, as Mach number decreases the shock will pass back over the wedge probe after it has passed over the conical probe. Small changes in the location of the shock with respect to the sensors can result in changes larger than those seen in the free-stream quantities due to the flow gradients (longitudinal and laterally) behind the U-shaped shock.

(a) Dryden F-15B with probes attached to CLIP.

(b) Close-up of probes attached to CLIP mounted under F-15B.

(c) Close-up of probe installation and CLIP looking downstream from under the aircraft.

Figure 21. Various photographs showing probe installation on NASA F-15B aircraft.

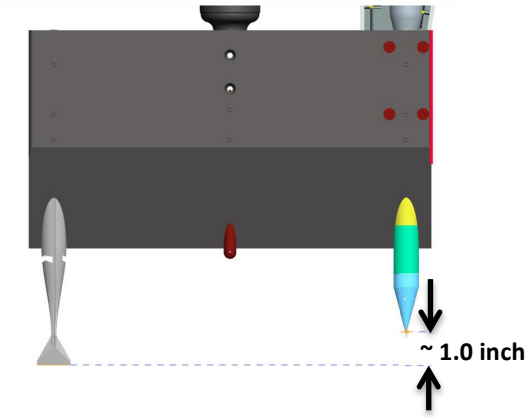


Figure 22. Sketch showing the difference in longitudinal location of wedge and conical probes.

## Results

In this section, measurements of the wind-tunnel, steady-state, free-stream flow variables are presented, as well as the longitudinally varying pressures due to the flow field created by the wall shock generator. These quantities are determined from the measured pressures and the data reduction equations in Appendices A and B.

Free-stream total and static pressure, free-stream Mach number and flow angle, are all determined by this process. In the case of the conical probe, a temperature measurement is also made inside the probe (see item 5 in fig. 12). With this measurement, free-stream velocity, temperature, density, and speed of sound may also be determined (noted earlier in section entitled “Description of New Wedge and Conical Probes”). Results of the flight tests, which were made with the sensors mounted on the CLIP, which, in turn, was mounted on the centerline of the lower surface of the F-15B, aircraft are also presented (see fig. 21).

The pressures are measured using cryogenic miniature pressure gages with ranges of 5 and 10 psi, depending on whether static or total pressures are being measured, respectively. They are claimed by the manufacturer to be temperature compensated from +100 °F down to -320 °F. The gages have a diameter of 0.066 inches and a length of 0.375 inches. The pressure gages with the 15° conical and wedge probes were calibrated at room temperature in a pressure chamber prior to and following the wind-tunnel tests. In addition, a series of pressure calibrations were performed in the wind tunnel during the no-flow pump-down phase, which ranged from atmospheric pressures to slightly below 3.0 psi, and the results correlated with the pressure-chamber calibration.

In flight, where the static temperatures at 45 to 50 thousand feet may be as low as -75 °F and the stagnation temperature (at M=2.0) as high as +240 °F, accurate pressure measurements require the temperature compensation capabilities that the gages are claimed to possess. Figure 23 shows calibrations, carried out at DFRC, for two 5-psi gages over temperatures from -50 °F to +140 °F. The calibration for the 5-psi gage used for the upper pressure port (see fig. 23a) on the conical probe shows a difference of ~3 percent between the 70 °F calibration and the -50 °F calibration at 5 psi pressure. The calibration of the gages used for the left side pressure port of the conical probe, shown in figure 23b, shows that the temperature is better compensated over the range where the calibration was made. The other gages used for the conical probe and the wedge probe show similar variations in temperature compensations. Later in this section, the effect the variances have on the determination of the free-stream flow variables of both the wind-tunnel and flight tests will be illustrated. In the case of the former, only wedge-probe data will be presented, since three of the pressure gages in the conical probe were replaced for the flight tests and no calibration data, at other than room temperatures, were available for the original pressure transducers used in the wind-tunnel tests. As a consequence of the lack of temperature compensation of the miniature pressure sensors, the original wind-tunnel data for the conical and wedge probes using room temperatures calibrations (~70 °F) are given in Appendix C.

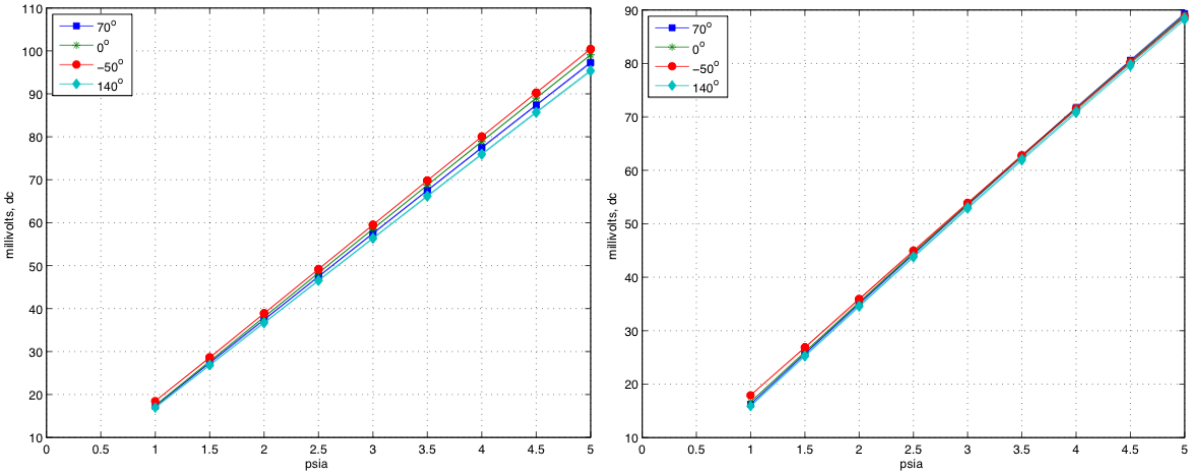


(a) Upper static-pressure gage on conical probe forebody. (b) Left-side static-pressure gage on conical probe forebody.

Figure 23. Calibration of two conical probe gages at four temperatures from -50 °F to 140 °F.

### *A. Wind-Tunnel Flow-Angle Measurements:*

Measurements were made at three nominal Mach numbers, 1.6, 1.8, and 2.0. The angle of attack was varied from -4° to +8°. Data for these three Mach numbers measured by the wedge probe are plotted in figure 24. Figure 24a, for a nominal Mach number of 1.6, shows that the differences with the wind-

tunnel data are not quite linear and that the 71 °F calibration data are generally below the wind-tunnel value while those for the 125 °F are above. It also shows that the difference in the 71 °F and 125 °F calibration causes about a one (1.0) degree difference in the calculated angle of attack. A similar result is seen in figure 24b for a Mach number of 1.8, but the variations are linear and the differences are smaller. At a Mach number of 2.0, both the 71 °F and 125 °F calibration data are above the wind-tunnel values with the 125 °F data being about a half-degree higher. Since the wind tunnel runs at temperatures near 125 °F, the data using the 125 °F calibration is the most accurate. The 71 °F calibration data for the wind-tunnel tests were obtained at a separate calibration facility near the wind tunnel facility. The 125° single-point calibration was obtained in the wind tunnel at a known temperature and pressure condition.

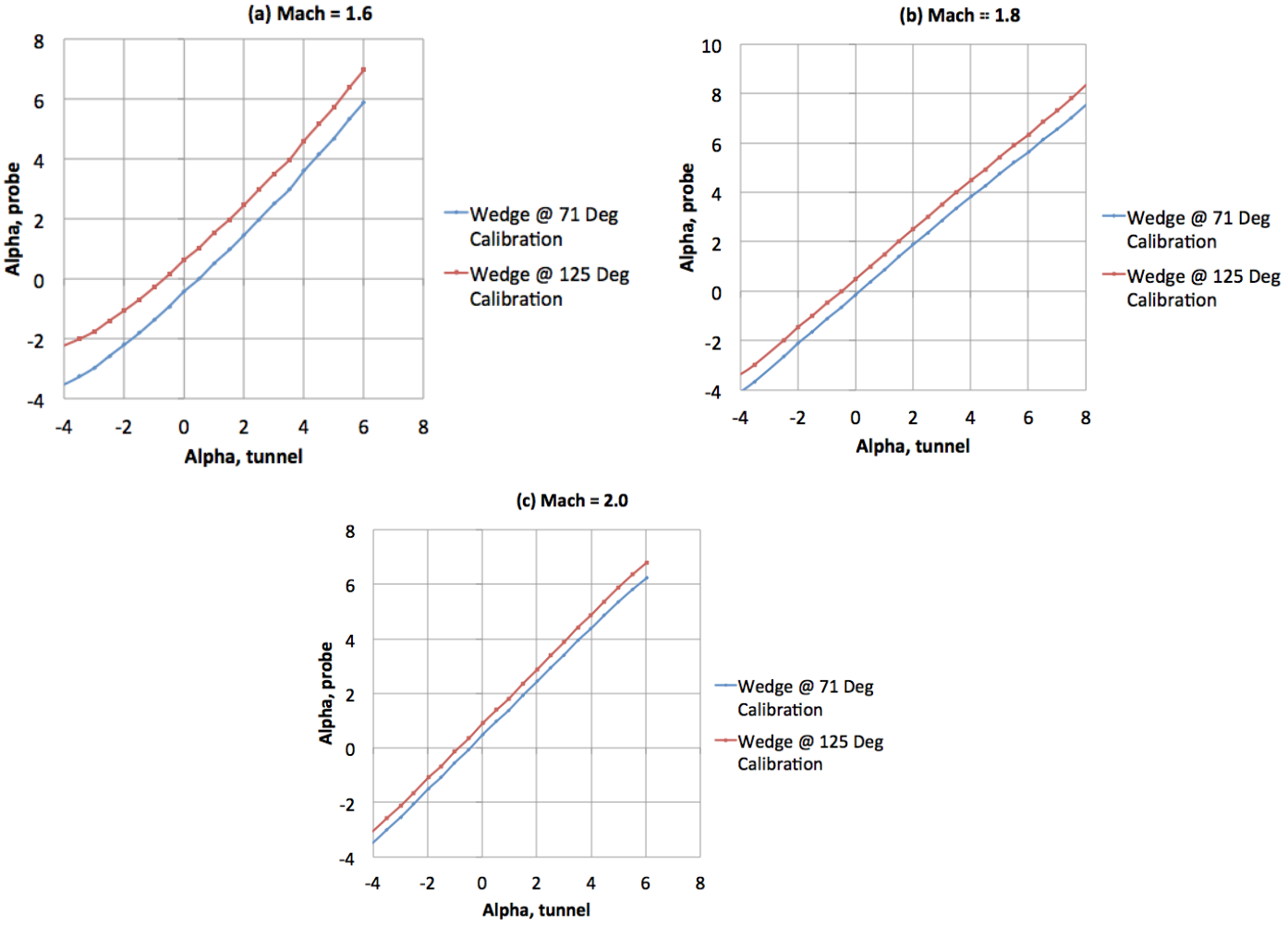


Figure 24. Comparison of wedge probe measured flow angle to wind-tunnel angle-of-attack setting for three Mach numbers.

### *B. Wind-Tunnel Static-Pressure Measurements:*

The data of most interest are the pressure data, since it is this quantity that is used to judge boom levels and it is used also in boom propagation codes. Figure 25 shows the static-pressure data for three nominal Mach numbers for the wedge probe as well as the 2° cone. It is obvious that the 71 °F calibration data are slightly less than the wind-tunnel data, while the 125 °F data yield larger values by 8 to 14 psf and are essentially the same as the 2° cone results.

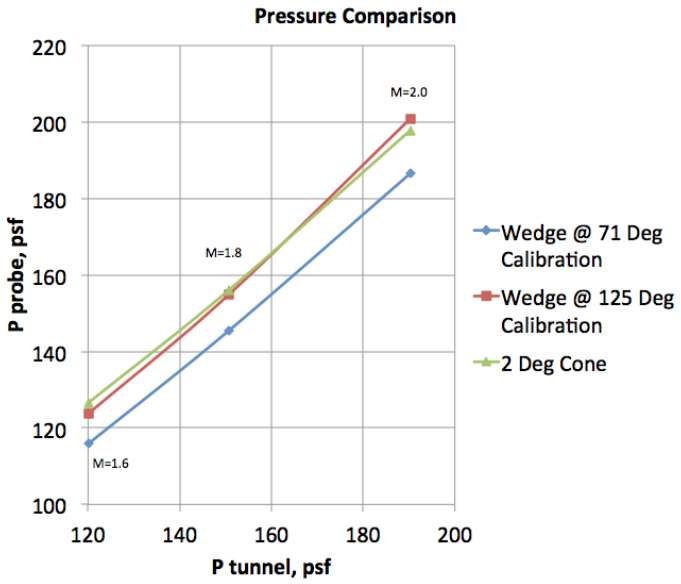


Figure 25. Comparison of wedge probe measured pressure to wind-tunnel values for three Mach numbers.

### *C. Wind-Tunnel Mach Number Measurements:*

Mach numbers determined by the wedge probe at zero angle of attack, using two different calibration temperatures, are plotted in figure 26 as a function of the wind-tunnel Mach number. The 71 °F calibration values for the wedge probe are higher than determined by the wind-tunnel system, while those for the 125 °F calibration are lower. The difference is about 0.05 Mach.

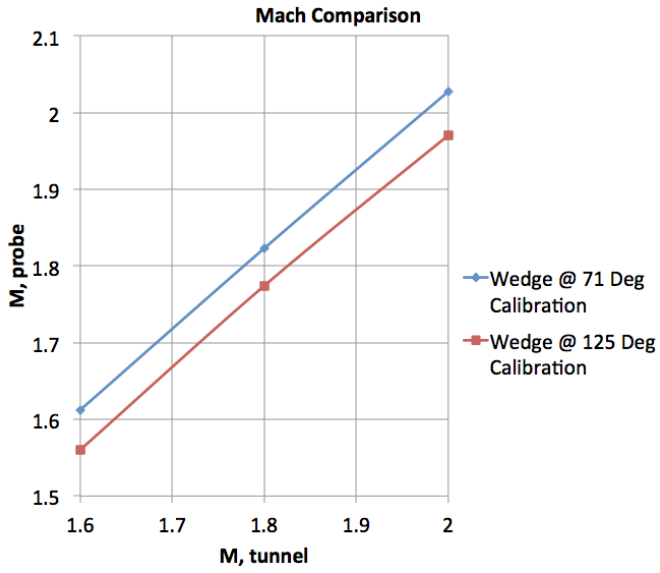


Figure 26. Comparison of wedge probe measured Mach number to wind-tunnel setting.

A comparison of the Mach numbers determined by the wedge probe using the 125 °F calibration with that determined by the 2° cone probe is given in figure 27. Clearly they are in close agreement. Note that the calculation of the Mach number for the 2° cone uses a total pressure measured upstream. Normally the 2° cone is not used to measure Mach number.

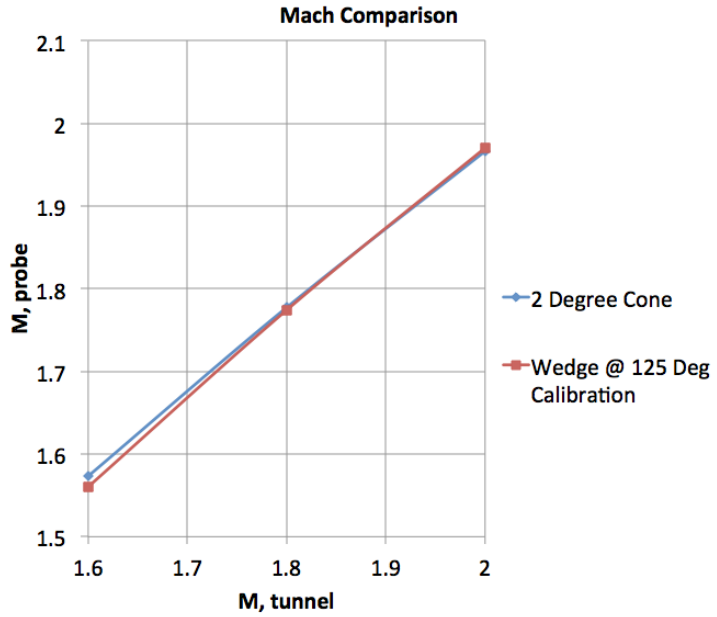


Figure 27. Comparison of Mach numbers measured by wedge probe and 2° cone with wind-tunnel measured Mach number.

### *D. Wind-Tunnel Longitudinally Varying Pressures due to Shock Generator:*

Pressure and Mach number distributions experienced by moving the wedge probe longitudinally through the flow field created by the shock generator (wall disturbance bump) over a distance of about 13 inches are discussed in this section. For this probe, the leading edge shock from the generator is encountered at an x of ~3.0 inches (see fig. 28) and it has a strength of ~0.32 psi relative to the free-stream pressure level. Note that the dip in pressure just ahead of the shock is due to the fact that all of the pressure orifices are not exposed to the shock at the same time and the equations produce an unrealistic result. In flight, where the sonic boom signatures are on the order of the length of the generating airplane, this is not a problem. The longitudinal distance between the free-stream total pressure tube on the bottom surface of the wedge and the total-pressure tube on the top surface is ~0.29 inches. Also, the shock off the leading edge of the disturbance bump is smeared by the wind-tunnel wall boundary-layer flow. Once all the pressure orifices experience the shock, it appears to have been resolved in 0.3 inches of travel. The bow shock is followed by a gradual pressure recovery. There is a slight increase in pressures starting around x = 5.5 inches which is due to the secondary shock generator (see Fig. 16).

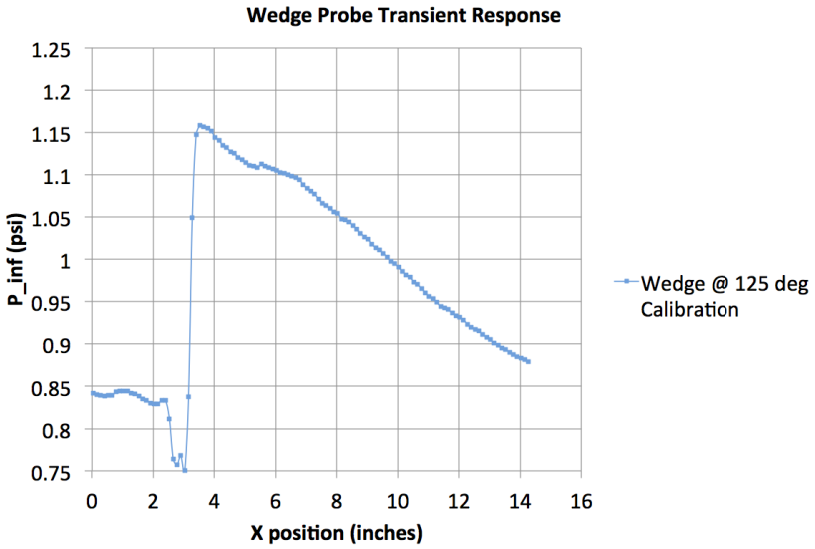


Figure 28. Response of wedge probe to disturbance-bump shock.

Figure 29 shows the pressure distribution, due to the shock generator (wall disturbance bump), measured by the 2° cone compared to the wedge probe measurement. Its pressure orifices are located about a half-inch ahead of the leading edge of the wedge probe, and thus it senses the shock jump ahead of the wedge probe by this amount. The gradual shock recovery downstream of the shock measured by the 2° cone has a lower gradient than the wedge probe and the values are lower than the wedge probe values out to an x position of 11 inches. It is not clear if this is a result of the variable flow field, and the effect it can have on the 1.4 inches of the 2° cone ahead of the pressure orifices, or the use of the tunnel-system total pressure measurement in the 2° cone calculation. It appears that this is a different phenomenon from the smearing of the abrupt shock jump that is seen in this figure, as well as that shown in figure 7.

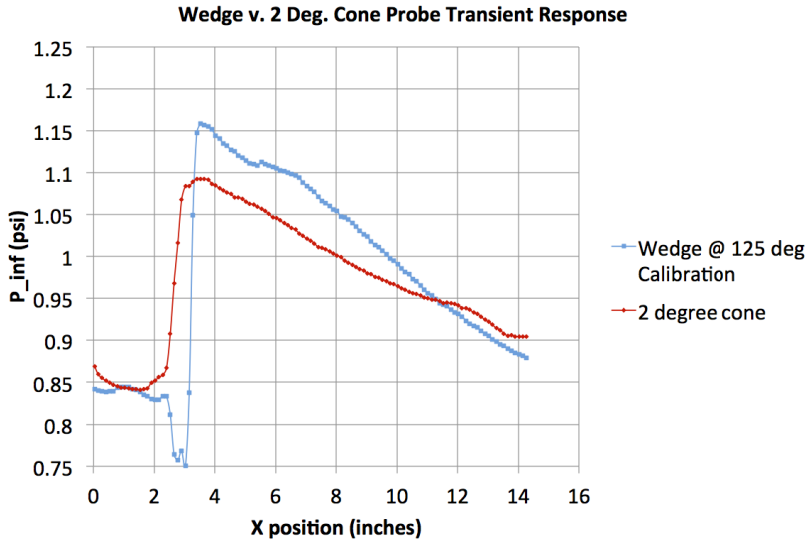


Figure 29. Response of wedge probe and 2° cone probe to disturbance bump shock.

### *E. Transient Measurements of Mach Number:*

The variation of Mach number with distance was determined by the wedge probe using both the 71 °F and 125 °F calibrations of the pressure transducers. Figure 30 shows the variation with x of the Mach number for these two calibrations. There is an increase in Mach number ahead of the shock jump due to the fact that all three pressure sensors are not exposed to the shock at the same time, as noted earlier. Behind the shock the Mach number drops abruptly to 1.8. It is followed by a Mach recovery that lasts out to the end of the measurements. Note that there is an inflection beyond at x of 5 that is thought to be due to the secondary shock generator.

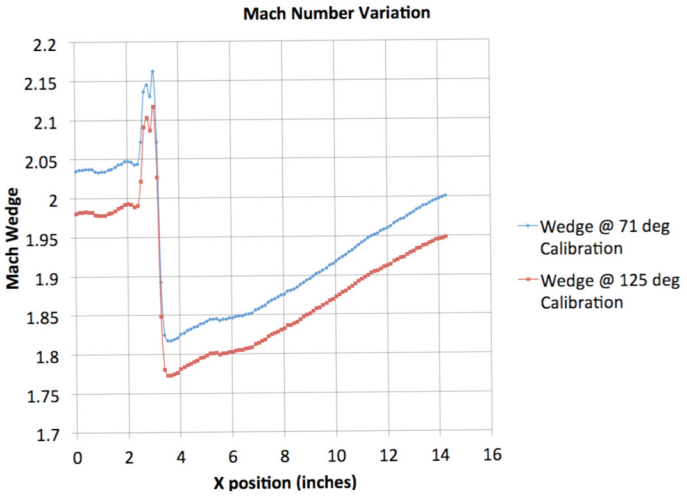


Figure 30. Effect of calibration temperature on the wedge probes's Mach number variation with x.

The magnitude of the Mach number measured using the 125 °F calibration is about 0.05 less than that calculated using the 71 °F calibration. Also, as noted earlier, the 125° calibration data are probably the most accurate, since the wind tunnel operates close to 125 °F.

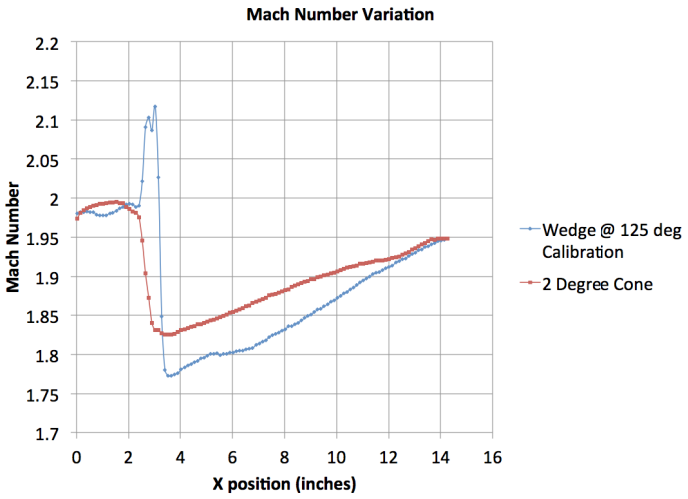


Figure 31. Comparison of wedge probe and 2° cone Mach number variation with x.

A comparison of the Mach number determined by the wedge probe using the 125 °F calibration to that of the 2° cone is shown in figure 31.

As with the pressure variations with the x position, the Mach gradients aft of the bow shocks are different, with the 2° cone's Mach variation with x having a smaller slope. Also, the 2° cone does not appear to sense the bump at an x of 5.5 inches. It is interesting that the two sensors produce about the same Mach number at an x of 14 inches.

***F. Temperature Measurements in the Conical Probe:***

The purpose of the temperature sensor inside the conical probe is to determine the free-stream stagnation temperature. To do this requires a measurement of the pressure in the channel ahead of the temperature sensor and the total pressure behind the normal shock at the apex.

These quantities are used in the equation

$$T_2 = \left(\frac{P_{tot}}{P_1}\right)^{2/7} T_{meas}$$

to calculate the stagnation temperature in the conical probe which is equal to that in the free stream.

Since the total pressure inside the cone was not measured accurately by the pressure sensor in the cup due to the fact that the flow velocity through the probe was too high (because of leakage), it was not possible to utilize the above equation as intended. Also, there was a problem of leaks through the joints and under the sleeve that is used to adjust the vent-hole size (see fig. 12). The temperature sensor used did not respond well to temperature changes and, in a changing wind-tunnel or flight environment, temperature was not accurately measured.

With no flow, or a trivial amount of flow through the conical probe, the pressure gage in the channel indicated a pressure equal to the stagnation value and the temperature gage read ~562 °R, which was exactly the free-stream stagnation temperature. So it clear that with a proper total-pressure measurement and flow velocity through the cone that the free-stream stagnation temperature could be determined as designed.

***G. F-15B Shock Systems and Data Presentation:***

The location of the conical and wedge probes attached to a fixture, referred to as the Center Line Instrumented Pylon (CLIP), under the fuselage of NASA's F-15B aircraft, is shown in figure 21. A sketch of the profile of this aircraft with major shocks emanating from the various components expected to produce significant shocks, is shown in figure 32. As can be seen, depending on whether the CLIP shock is ahead of, or behind, the probes there will be at least three or four significant shocks ahead of the probes. Thus, there is no possibility that the probes there can measure anything representative of true aircraft free-stream quantities. There are, however, measurements of the free-stream quantities by the airplane flight-test noseboom and total temperature probe. Comparisons can be made to show the differences between these free-stream quantities and those measured by the probes.

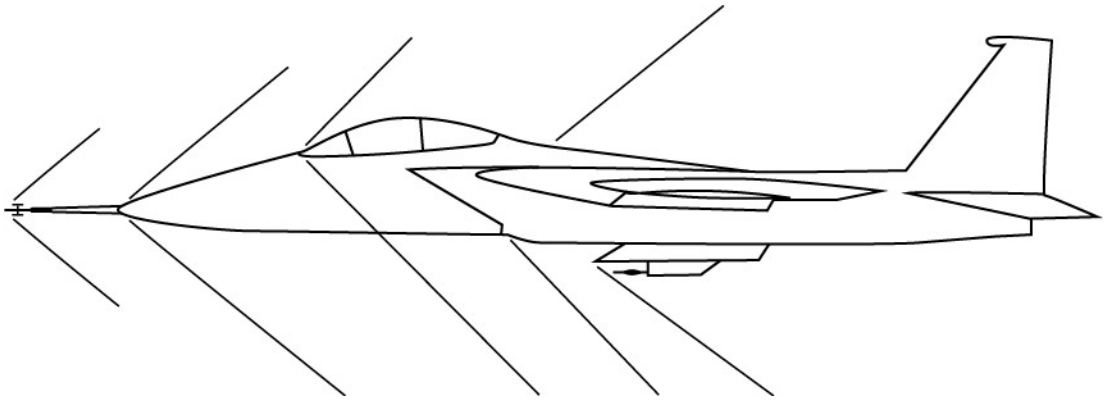

Figure 32. Sketch of the F-15B aircraft showing the shocks off the various aircraft components ahead of the CLIP.

Five test flights were made with different orientations of the wedge and conical probes on each flight. Table 1 below shows these orientations looking from in front of the probes along with the flight number designations for each of the five flights.

**Table 1: Flight Test Program**

| Flight | Date (2011) | Probe Orientation Looking from Front* |
|---|---|---|
| 406 | March 25 | — T  O T |
| 407 | March 29 | T T  — O |
| 408 | March 30 | T\|  T O |
| 409 | March 31 | O T  — T |
| 410 | April 1 | O T  \| T |

— = wedge probe

O = conical probe

T = top of probe

*T indicates orientation of probes. In flight 406, for example, the probes were mounted upside down and their top sides were on the bottom.

The subsequent data presentation will utilize data from flights 406, 407, and 409. As can be seen from the table, in flight 407 the probes were inverted from the flight 406 orientation and in flight 409, the two probes switched locations from that of flight 406.

Note that the general flow direction at the test location is downward, so the probes in the inverted position (top down) are in the preferred orientation with respect to the local flow.

***H. Sensitivity of Data to Calibration Temperature of Pressure Gages:***

As noted in the introduction to this "Results" section, some of the pressure sensors were not adequately compensated for temperature changes. Thus, the magnitude of the calculated flow variables will change depending on the temperature of the calibration used. To illustrate this fact, the calculated Mach number, static-pressure, and total-pressure variations with time for flight 406, for 70 $^{o}$F and -50 $^{o}$F

calibrations, and for both the conical and wedge probes are given in figures 33 and 34, respectively. Also shown in figures 33 and 34 are the airplane nose boom measurements of the free-stream quantities. Figure 33a shows the Mach number determined by the conical probe for both the 70 °F and -50 °F pressure sensor calibration. The figure shows that the Mach number for both calibrations is less than free stream, as expected. The -50 °F calibration yields higher values of Mach number than the 70 °F calibration. At a Mach number of ~1.85 the -50 °F result is ~2.0 percent higher than the Mach number calculated using the 70 °F calibration. Note that there is a shock passage over the gage at a time of ~135 seconds and another at ~330 seconds. Both occur between Mach numbers of ~1.4 and 1.6.

Static-pressure measurements for the conical probe are plotted in figure 33b. Here, the 70 °F calibration is shown to yield higher values of static pressure for Mach numbers greater than 1.6 than for the -50 °F calibration by about 5 percent. Total-pressure variations with time (see fig. 33c) for the 70 °F and -50 °F calibration agree fairly well, with a difference between the two at the maximum value of ~2.0 percent.

The effects of calibration temperature on the calculated flow quantities for the wedge probe are shown, as noted, in figure 34. As with the conical probe, figure 34a shows that the -50 °F calibration yields the higher values of Mach number with values about 5.5 percent higher in the area of the maximum Mach number. Note that there appears to be a shock passage starting just beyond 250 seconds and lasting to ~310 seconds when, in fact, the top or short total-pressure gage was saturated beyond 10 psi (see fig. 34c). This was a result of calibrating the 10-psi gages to 10 psi, when actually they are capable of accurate measurement beyond this value.

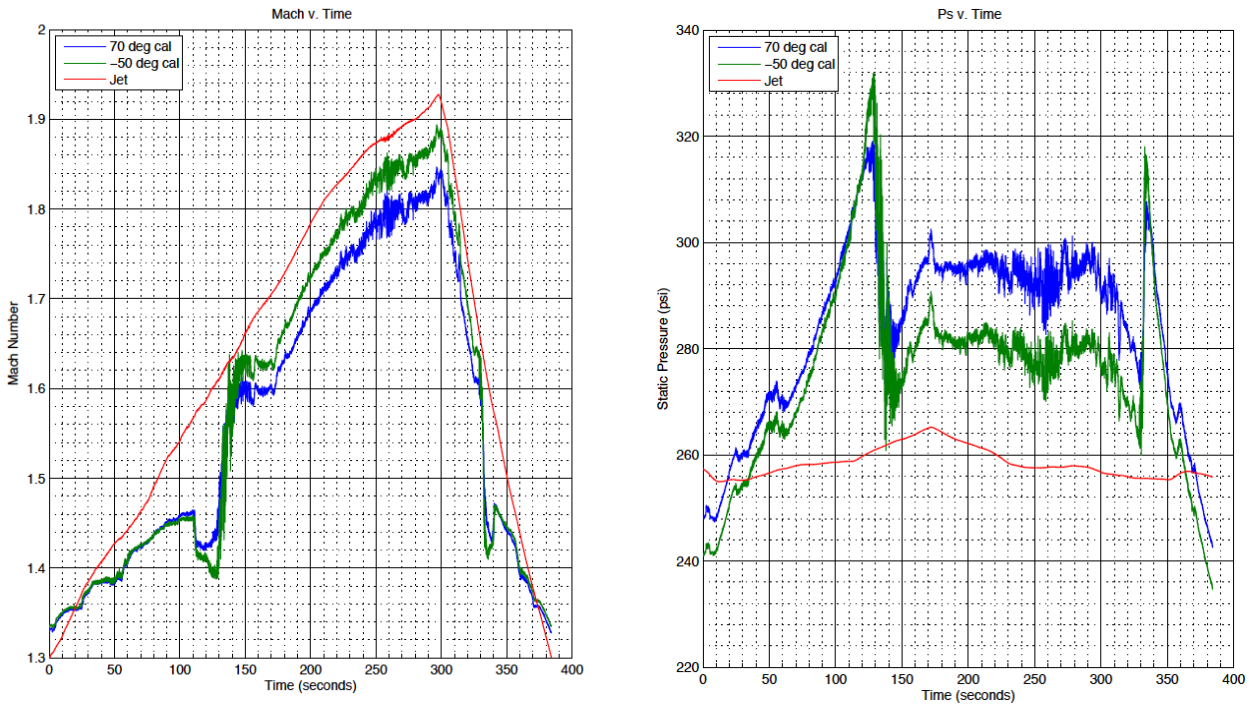


(a) Mach number.

(b) Static pressure.

Figure 33. Comparison of computed time variations of flow variables for the conical probe using pressure sensor calibrations for 70 °F and -50 °F as well as aircraft (jet) measured quantities.

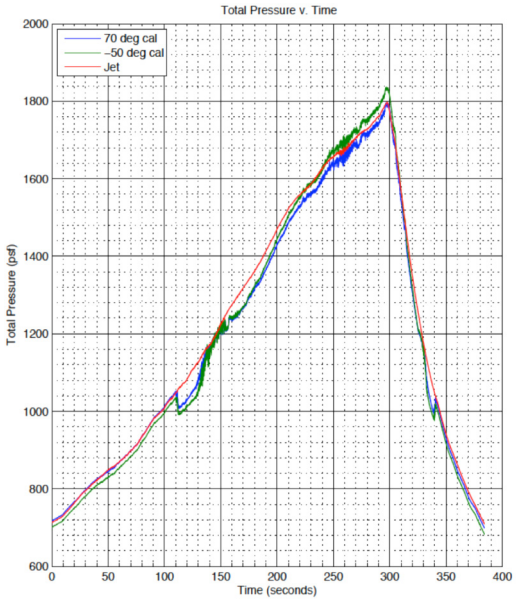


(c) Total pressure

Figure 33. Concluded.

The static pressure variation with time for the two calibration temperatures, shown in figure 34b, show the -50 °F calibration to yield much lower values. The time variations are also different from the conical probe, apparently due to the more forward location of the wedge probe or flow asymmetry. Total pressures for the two calibrations, figure 34c, are only about 3 percent different at the maximum value.

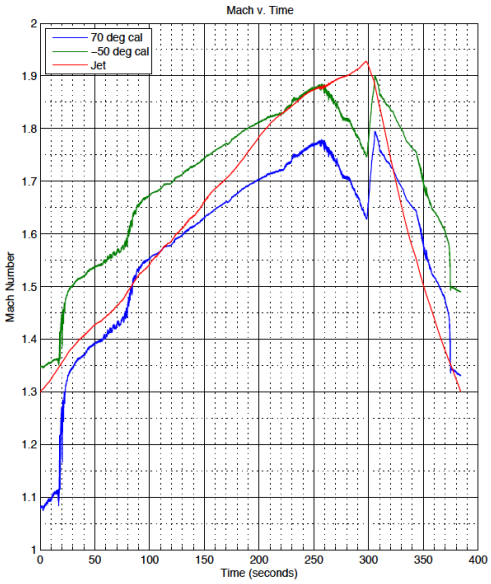


(a) Mach number.

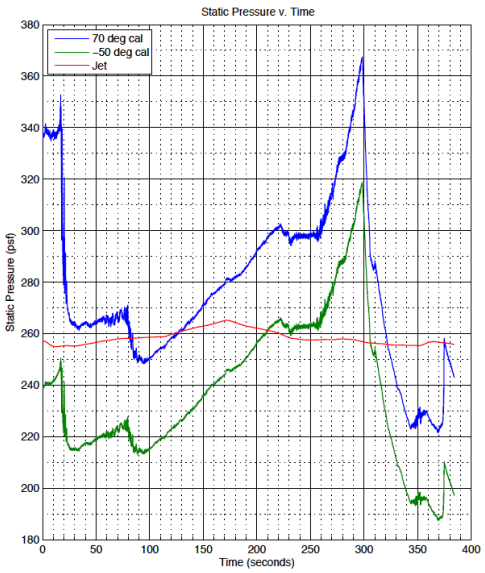


(b) Static pressure.

Figure 34. Comparison of computed time variations of flow variables for the wedge probe using pressure sensors calibrations for 70 °F and -50 °F. Flight 406.

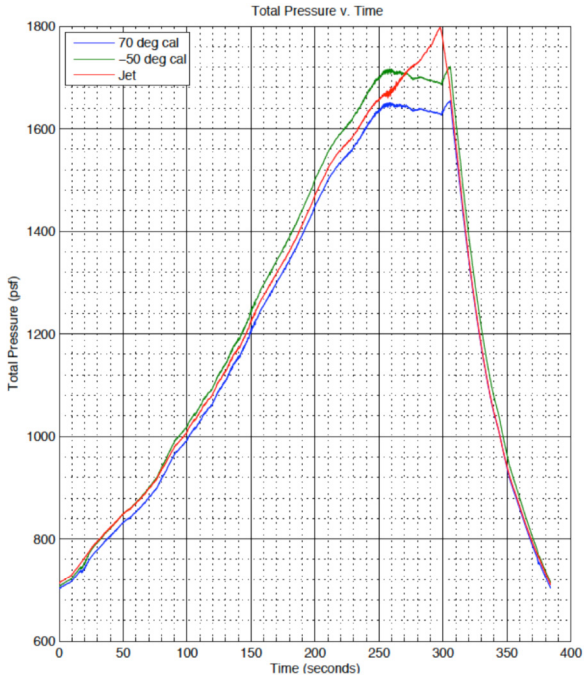


(c) Total pressure.

Figure 34. Concluded.

To further illustrate the effect of the gage-calibration temperature, angle of attack, calculated using all four temperature calibrations, is plotted as a function of Mach number in figure 35. Figure 35a gives the data for acceleration phase of the flight and figure 35b for deceleration. Clearly the difference between the 140 °F calibration and the -50 °F calibration are large and vary ~3 degrees at Mach 1.8 up to 6 degrees at Mach 1.4 during acceleration.

The acceleration and deceleration phase test points were performed at the same constant altitude. While the acceleration phase was performed in afterburning power, the deceleration phase was performed at military power (maximum non-afterburning) due to a lockout feature which does not allow less than military power (on these particular engines) at higher supersonic conditions (M > 1.4). There is no appreciable difference in inlet flow between military and afterburning power settings. This is important because the inlet flow, which has a significant effect on the test area flow, would be essentially the same for both phases. Based on this information the flow at the test area would be expected to be nearly the same for both the acceleration and deceleration phases. The significant difference between the two flight phases is the temperature at the sensors. Prior to the acceleration phase, the gages and surrounding structure had been cold-soaked to approximately -70 °F or colder for at least 10 minutes. During the acceleration, the gages and structure would have warmed significantly due to the aerodynamic heating, especially at the higher Mach numbers. During the deceleration phase the gages would be expected to be significantly warmer than during the acceleration phase.

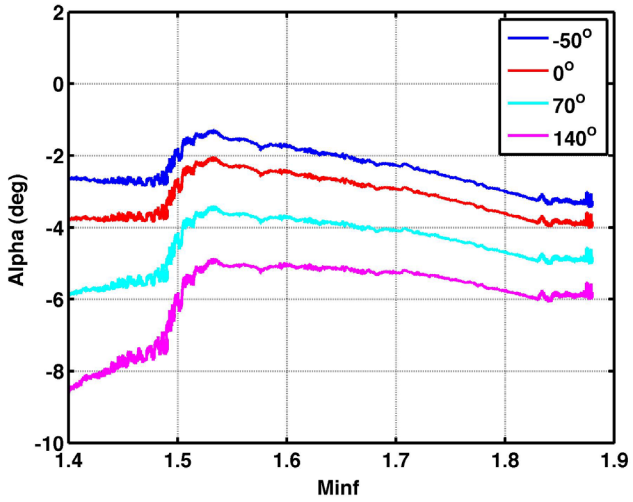


(a) Alpha wedge comparison flight 406 acceleration.

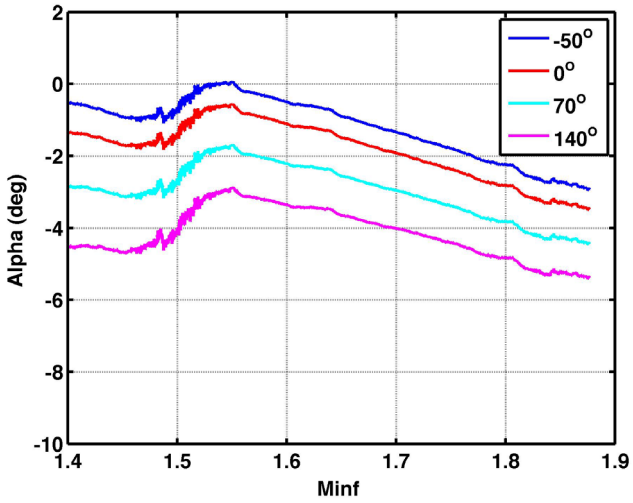


(b) Alpha wedge comparison flight 406 deceleration.

Figure 35. Wedge probe local alpha versus free-stream Mach number for a set of representative temperatures and for acceleration and deceleration portions of flight 406.

If one uses an interpolation scheme with the four calibrations available, and the temperature measured by the temperature gage in the conical probe, then the possibility of reducing the error, or uncertainty, in the calculated flow variables would seemingly be enhanced. While the temperature gage is not located where the pressure sensors are, and there is some lag in the measurement of the changing environment, it should yield results better than using a single constant-temperature calibration. Figure 36 shows the results of such an exercise for both the acceleration and deceleration phases of flight 406. The improvement is clear and lends credit to the possibility that if one has calibrations for a range of temperatures and an accurate temperature measurement where the transducers are located, then accurate data will be produced. Ideally, one would like to have fully temperature-compensated gages, and then no temperature measurement would be required.

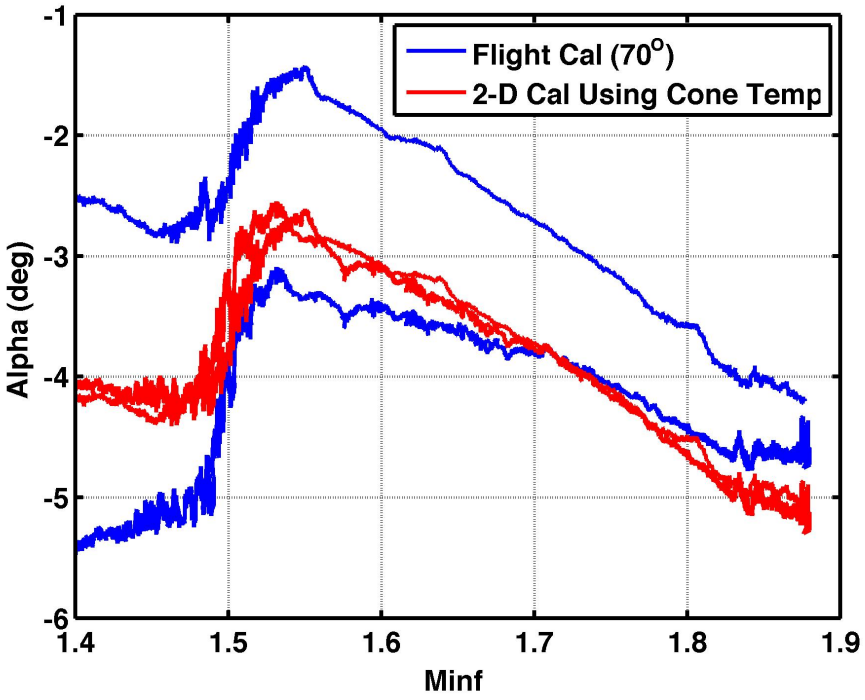


Figure 36. Wedge probe local alpha versus free-stream Mach number by using an interpolative 2-dimensional calibration (pressure and temperature). Note: Cone Temp in figure refers to conical probe temperature.

### *I. Comparison of Wedge and Conical Probe Data:*

It is evident from figures 33 and 34 that the wedge-probe results are more affected by temperature than the conical probe. Thus, when results from the two probes are compared, the differences in magnitude may not be accurate. However, differences in the variations with time are significant and are due to the approximately 1.0 inch more forward location, as well as the higher resolution of the wedge probe. Also note that there is some significant asymmetry in the local flow. In a subsequent figure, data from flight 407 using the -50 °F calibration data will illustrate some of these effects.

Mach number data for flight 407 (see fig. 37a) shows the earlier time passage of the shocks off the CLIP edges over the wedge probe at ~116 seconds versus that for the conical probe at 150 seconds. Passage of these shocks in the other direction occurs at 320 seconds and 350 seconds for the conical and wedge probes, respectively. There is also the pressure-gage saturation problem that starts around 250 seconds and lasts until ~ 300 seconds (see figs. 37 a, c, d, and e). Presumedly the 10-psi gages in the conical probe were just below the saturation value. Recall that the static- and total-pressure data shown in figures 37 c and d are calculated values of the upstream flow. This is why the saturation of one total-pressure gage on the wedge probe causes a large anomalous change in static pressure (fig. 37c) when the static-pressure gage is not saturated.

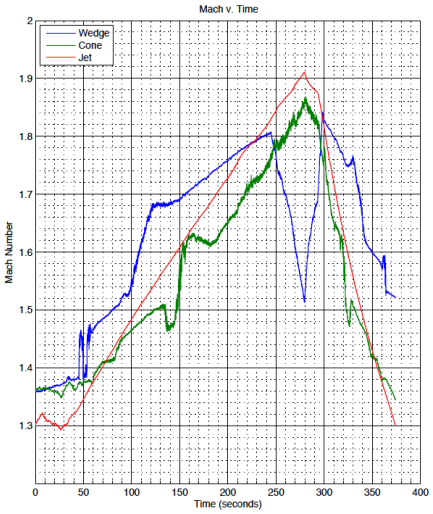


(a) Mach number.

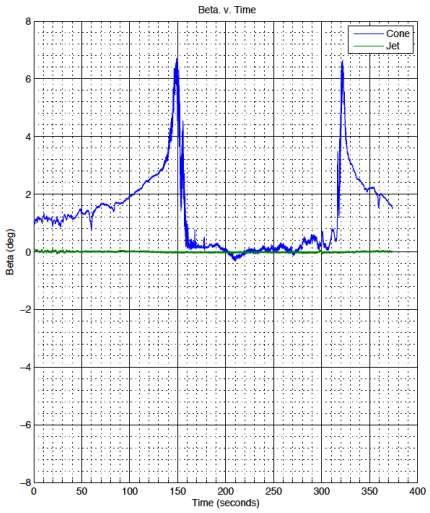


(b) Angle of sideslip.

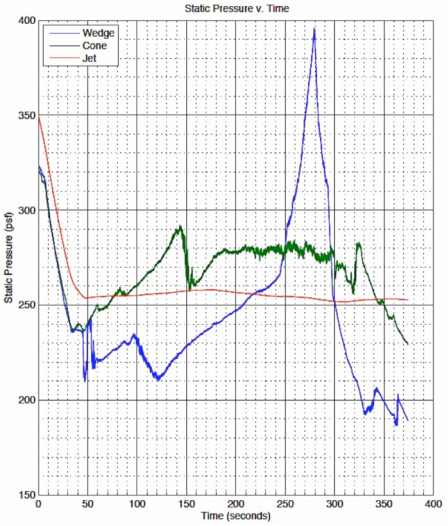


(c) Static pressure.

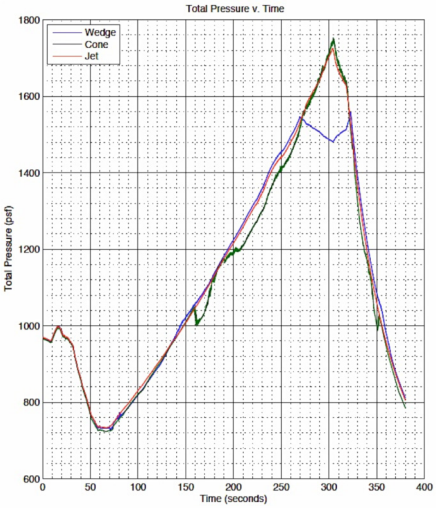


(d) Total pressure.

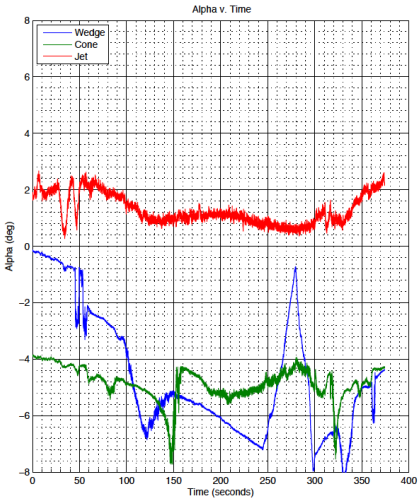


(e) Angle of attack.

Figure 37. Comparison of computed time-variation of flow variables for the wedge and conical probes using the -50 °F calibration of the pressure sensors for flight 407.

The conical probe measures sideslip, or β, angle in addition to angle of attack; the wedge probe does not. The only angle being measured by the wedge probe is the local flow angle in the vertical plane by the wedge. Figure 37b, again for flight 407, shows this measurement as a function of time. Noteworthy in this figure is the large change or spikes in the β angle as the shock off the edge of the CLIP passes.

Static pressure differences between the wedge and conical probe measurements are evident in figure 37c. In addition to the changes that occur during shock passage, the higher level of static pressures measured by the wedge probe versus those of the conical probe between the times of 250 and 300 seconds are due to the saturation of the 10-psi top or short total pressure gage. With the exception of the changes due to shock passage and the aforementioned wedge probe total sensor saturation, the computed total pressure is essentially the same for the two probes (see fig. 37d) consistent with the physics of fluid flow where no energy has been added or subtracted.

The angle of attack for the two probes is plotted in figure 37e. The differences mirror those of Mach number where the shock passage at times of 100 and 150 seconds produce spikes in the variation of angle of attack.

***J. Temperature Variations:***

Flight measurements of temperature inside the conical probe, labeled $T_{measured}$ in figure 38, are converted to stagnation temperature, $T_2$, using the equation in Section F and the total pressure at the cone apex and the static pressure measurement in the channel of the temperature sensor (see fig. 38). Since the stagnation temperature inside the cone ($T_2$) is the same as in the free-stream stagnation temperature ($T_S$), it is possible to calculate free-stream static temperature ($T_{inf}$) using

$$T_{inf} = \frac{T_S}{1 + \left(\frac{\gamma - 1}{2}\right) M_\infty^2}$$

and the local Mach number determined earlier. Note that the term “free stream” above means the flow just ahead of the conical probe and not that ahead of the airplane. Also, it is important to recognize that as the flow is processed by the shocks ahead of the CLIP (see fig. 32), they cause an increase in static temperature. So the fact that $T_{inf}$ is higher than that of the airplane, labeled Jet, is no surprise. It is not entirely clear why there is such an increment between the jet total temperature and that determined by the conical probe. The ratio of the total pressure to the static pressure inside the conical probe is greater than 5 at the highest Mach tested number. The desired ratio (see fig. 10) was assumed to be approximately 1.001. This large difference accounts for the high stagnation-temperature values inside the conical probe and consequently the high calculated static temperature. It appears that there is too little flow through the conical probe as configured for flight (total pressure outside with annulus for internal flow). With the accurate determination of the Mach number and temperature just ahead of the conical probe, the speed of sound, velocity, and density could also be calculated. The time derivative of the velocity will give acceleration.

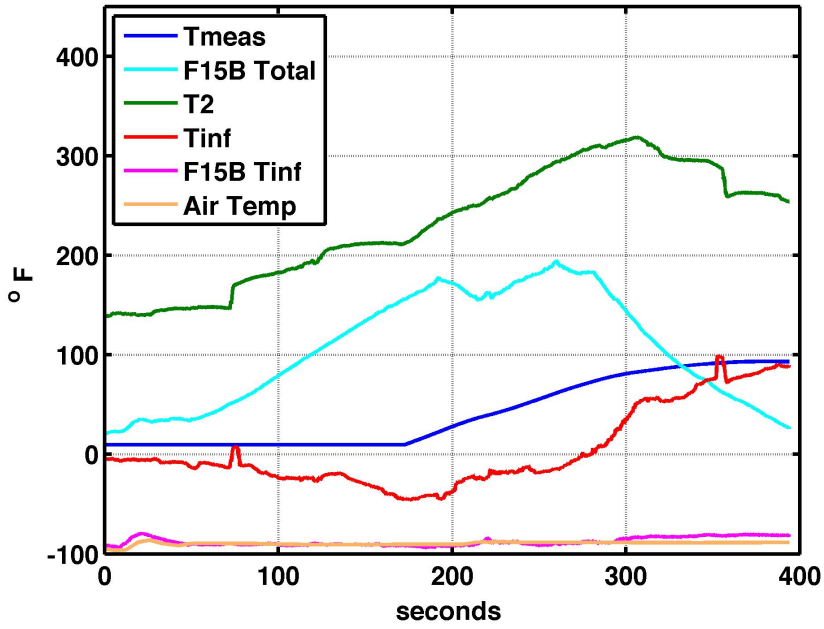


Figure 38. Variation of the temperature with time inside ($T_{meas}$ and $T_2$) and ahead of the conical probe ($T_{inf}$), as well as those in the air ahead of the F-15B (Air temperature) and behind the bow shock off the front of the F-15B aircraft. Flight 409.

The thin horizontal line at the bottom of figure 38, labeled air temperature, was obtained from a weather balloon on the day of flight 409. It is near constant, since the time period of these measurements was on the order of five minutes and the altitude changed very little.

## Summary Remarks

Conical and wedge probes designed to provide for near instantaneous measurements of free-stream flow variables have been tested in the wind tunnel and in flight. Wind-tunnel tests were carried out in the NASA Langley Research Center's Unitary Plan Wind Tunnel and the flight tests on a fixture attached to the lower fuselage of a NASA Dryden Flight Research Center F-15B aircraft. These tests were termed functional, check-out, or structural-integrity tests. Free-stream measurements were made in the wind-tunnel tests successfully, while the flight tests, because of the location of the probes, only allowed the measurement of the local flow variables ahead of the probes.

As expected, the wedge probe provided the most accurate data. The close proximity of its sensors made for the least smearing of the gradients of all the flow quantities. In both the wind-tunnel and flight tests the problem of leaks at the back of the conical probe and other flow issues (annulus in flight) caused the flow velocity over the temperature sensor inside the conical probe to be uncertain (appeared excessive during wind-tunnel tests and inadequate during flight tests). Nevertheless, the internal measurements effected by this flow were used to determine the total temperature inside the conical probe and, consequently, in the free stream.

### Wind-Tunnel Tests

The conical-probe measurements were hampered by the total pressure not being accurately measured by the sensor located inside the probe itself. The use of the total pressure measured by the wedge probe

for the total pressure at the cone enabled the calculation of the flow quantities of interest using the static pressures on the cone. However, there are gradients of all the flow quantities in the test section, as noted in the paper, and with the wedge and conical probes separated laterally by 10 inches the accuracy of the conical probe calculations will incur a small error due to the use of the wedge probe's total-pressure measurement. This error is also of particular concern when the total pressure (from the wedge probe) is used in combination with the static pressure in the channel containing the temperature sensor to correct the measurements made by the temperature sensor to yield the stagnation temperature. As noted in the section entitled "Description of New Wedge and Conical Probes," the total-pressure measurement was moved from the cup inside the probe to the apex of the cone for the flight tests.

The smearing of the transient variations of pressure and Mach number with longitudinal distance for the 15° conical probe and the 2° cone is greater than the wedge probe, as noted, but in the case of the former this phenomena is caused by the size (diameter) of the probe which enables the inclusion of the temperature sensor. In the flight environment where aircraft and their sonic boom signatures are 50 or 100 feet in length or more, this is not a problem. For the 2° cone, which is only used in wind-tunnel measurements, the smearing is less for large models than for small. There is a built-in error, however, due to the pressure orifices being on the surface of a 2° cone and its shock flow field as well as the boundary layer on its surface.

Overall there is not enough data to make a consistent story between the flow-angle measurements of reference 24 (wind-tunnel calibration data) and the flow-angle measurements of the probes.

## Flight Tests

The flight tests were carried out successfully with five flights being conducted. Anomalies between the data taken during acceleration and data taken during deceleration of the same flight highlighted the effects that temperature had on the calculated quantities. Further analysis showed that using the room-temperature calibrations for the miniature pressure transducers were the problem, since adequate compensations for the lower temperatures were not being done. Subsequent calibrations of the nine pressure sensors for temperatures of -50 °F, 0 °F, 70 °F and 140 °F showed that some gages were fairly well compensated and others were not. Use of these calibrations showed that significant differences occurred between the calculated flow variables at 70 °F and -50 °F. Figures included in the paper show these differences and point out the need for an accurate temperature measurement where the miniature pressure sensors are located, along with calibrations for a range of temperatures, or, ideally, sensors that are truly temperature compensated. A third possibility is to house the sensors in a temperature-controlled enclosure.

## Future Tests

The conical and wedge probes were intended to be located in front of the aircraft fuselage so that actual free-stream flow variables can be measured. Improvements to the conical probe, including the use of a faster responding temperature gage and appropriate sizing of inlet and exit area to control the flow through the probe, would result in better measurement of temperature and response to temperature change. With these improvements it appears that the conical probe would be capable of providing for more accurate measurement of total temperature and the free-stream quantities that depend on this measurement. Also, more accurate calibrations and temperature compensation of the pressure transducers, along with an understanding of the effect of the local environment on the calibrations will lead to more accurate pressure measurements.

# References


1. Bobbitt, Percy J.; and Darden, Christine M.: A Wedge Shaped Supersonic Flow Field Probe. High Speed Research Sonic Boom, Vol. II. NASA CP 10133, May 1993.
2. Taylor, G. I.; and Maccoll, J. W.: The Air Pressure on a Cone Moving at High Speeds. I and II. Proc. Royal Soc. (London) Sec. A, Vol. 139, No. 838, Feb. 1933.
3. Maccoll, J. W.: The Conical Shock Wave Formed by a Cone Moving at a High Speed. Proc. Royal Soc. (London) series A Vol. 159, No. 898, April 1. 1937.
4. Staff of Ames 1-by-30 foot Supersonic Wind Tunnel Section: Notes and Tables for use in the Analysis of Supersonic Flow. NACA TN 1428, 1947.
5. Moeckel, W. E; and Connors, J. F.: Charts for the Determination of Supersonic Air Flow Against Inclined Planes and Axially Symmetric Cones. NACA TN 1373, 1947.
6. Stone, A.H.: On Supersonic Flow Past a Slightly Yawing Cone. II Jour. Math. and Phys. Vol. XXX, No. 4, Jan. 1952.
7. Massachusetts Institute of Technology, Dept. of Elec. Eng., Center of Analysis. Tables of Supersonic Flow Around Cones at Large Yaw by the Staff of the Computing Section Under the Direction of Zdenek Kopal. Tech. Rept. No. 5, Cambridge, 1949.
8. Ames Research Center Equations, Tables and Charts for Compressible Flow. NASA Report 1135, 1953.
9. Ferri, Antonio: Elements of Aerodynamics of Supersonic Flows. The MacMillan Company, New York, 1949.
10. Cubbison, Robert W.; and Melearson, Edward T.: Water Condensation Effects of Heated Vitiated Air on Flow in a Large Supersonic Wind Tunnel. NASA TM X-1636, 1968.
11. Gorlin, S.M.; and Slezinger: Wind Tunnels and Their Instrumentation. NASA TTF-346, 1966.
12. Bryer, D. W.: Pressure Probes Selected for Three-Dimensional Flow Measurements. ARC Rep. and Mem., No. 3037, 1958.
13. Carlson, Harry W.: Measurements of Flow Properties in the Vicinity of Three Wing-Fuselage Combinations at Mach Numbers of 1.61 and 2.01. NASA TM-64, 1959.
14. Putnam, Lawrence E.; and Capone, Francis J.: Experimental Determination of Equivalent Solid Bodies to Represent Jets Exhausting Into a Mach 2.20 External Stream. NASA TN D-5553, Dec. 1969.
15. Carlson, Harry W.; and Mack, Robert J.: A Wind-Tunnel Study of the Applicability of Far-Field Sonic-boom Theory to the Space Shuttle Orbiter. NASA TP 1186, June 1978.
16. Carlson, Harry W.: Correlation of Sonic-Boom Theory With Wind-Tunnel and Flight Measurements. NASA TR R-213, Dec. 1964.
17. Carlson, Harry W.; Mack, Robert J.; and Morris, Odell A.: A Wind-Tunnel Investigation of the Effect of Body Shape on Sonic-Boom Pressure Distributions. NASA TN D-3106, Nov. 1965.
18. Miller, David S.; and Morris, Odell A.: Wind-Tunnel Investigation of Sonic-Boom Characteristics of Two Simple Wing Models at Mach Numbers from 2.3 to 4.63. NASA TN D-6201, April 1971.
19. Shrout, Barrett L.; Mack, Robert J.; and Dollyhigh, Samuel M.: A Wind-Tunnel Investigation of Sonic-Boom Pressure Distributions of Bodies of Revolution at Mach 2.96, 3.83 and 4.63. NASA TN D-6195, April 1971.
20. Carlson, Harry W.; and Mack, Robert J.: A Study of the Sonic-Boom Characteristics of a Blunt Body at a Mach Number of 4.14. NASA TP 1015, Sept. 1977.
21. Mack, Robert J.; and Darden, Christine M.: Wind-Tunnel Investigation of the Validity of a Sonic-Boom-Minimization Concept. NASA TP 1421. Oct. 1979.
22. Carlson, Harry W.: An Investigation of the Influence of Lift on Sonic-Boom Intensity by Means of Wind-Tunnel Measurements of the Pressure Fields of Several Wing-Body Combinations at a Mach Number of 2.01. NASA TN D-881, July 1961.

23. Carlson, Harry W.: An Investigation of Some Aspects of the Sonic Boom by Means of Wind-Tunnel Measurements of Pressures About Several Bodies at a Mach Number of 2.01. NASA TN D-161, December 1959.
24. Jackson, Charlie M., Jr.; Corlett, William A.; and Monta, William J.: Description and Calibration of the Langley Unitary Plan Wind Tunnel. NASA TP-1905, Nov. 1981.

# Appendix A

## Data Reduction Equations and Solution Procedure Required to Derive the Free-stream Variables for the Wedge Probe

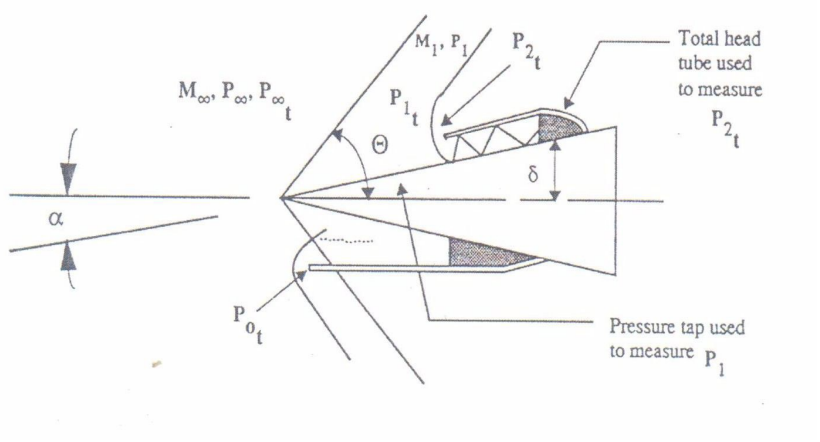


Figure A1. Wedge probe details and flow variables.

$M_\infty$, $P_\infty$, and α are flow quantities that the probe is required to determine.

$P_1$, $P_{o,t}$, and $P_{2,t}$ are measured (see sketch).

$M_1$ is calculated from $P_1$ and $P_{2,t}$.

With $P_1$, $P_{o,t}$ and $M_1$ known, $M_\infty$, Θ, $P_\infty$, and α can be calculated using the iterative procedure described below.

Procedure:

1. Measure $P_1$, $P_{o,t}$, and $P_{2,t}$

2. Calculate $M_1$ from

$$\frac{P_1}{P_{2,t}} = \left(\frac{7M_1^2 - 1}{6}\right)^{5/2} \left(\frac{5}{6M_1^2}\right)^{7/2}$$

See the discussion at the end of this Appendix for the iterative procedure for calculating $M_1$.

3. With $M_1$ and $P_1$ known, calculate $P_{1,t}$ from

$$\frac{P_{1_t}}{P_1} = \left(\frac{M_1^2 + 5}{5}\right)^{7/2}$$

4. Using oblique shock reactions, one can write

$$\frac{P_{1,t}}{P_1} = \left[\frac{(6\xi + 1)(M_\infty^2 + 5)}{5\xi(\xi + 6)}\right]^{\frac{7}{2}}$$

or solving for $M_\infty^2$

$$M_\infty^2 = \frac{5\xi(\xi + 6)}{6\xi + 1}\left(\frac{P_{1,t}}{P_1}\right)^{\frac{2}{7}} - 5$$

with $\xi = \frac{P_1}{P\infty}$

5. Make an initial guess for ξ using the curve fits for solutions to oblique shock relations found in reference 3 for the selected semi-wedge angle of 8°, $\xi = 1.41625 - 0.04M_{\infty,f} + 0.055M_{\infty,f}^2$ where

$$M_{\infty,f} = 72 - \sqrt{5161.538 - 153.846M_1}$$

6. With the first guess for ξ (=$\xi_1$) calculate $M_{\infty,1}^2$ from

$$M_{\infty,1}^2 = \frac{5\xi_n(\xi_n + 6)}{6\xi_n + 1}\left(\frac{P_{1,t}}{P_1}\right)^{\frac{2}{7}} - 5 \tag{1}$$

7. Then calculate

$$\left(\frac{P_1}{P_{o,t}}\right)_n = \frac{5\xi_n}{6M_{\infty,n}^2}\left(\frac{35M_{\infty,n}^2 - 5}{36M_{\infty,n}^2}\right)^{2.5} \tag{2}$$

If

$$\left|\left(\frac{P_1}{P_{o,t}}\right)_E - \left(\frac{P_1}{P_{o,t}}\right)_n\right| > 0.000001$$

from experiment

then calculate the next guess of ξ from

$$\xi_{n+1} = \xi_n + \frac{\left[\left(\frac{P_1}{P_{o,t}}\right)_E - \left(\frac{P_1}{P_{o,t}}\right)_n\right]}{2\left(\frac{P_1}{P_{o,t}}\right)_E}$$

and substitute it in from equation (1) for the new $M_{\infty,n}$, which in turn is substituted into equation (2) above and the check is repeated.

8. If $\left|\left(\frac{P_1}{P_{o,t}}\right)_E - \left(\frac{P_1}{P_{o,t}}\right)_n\right| > 0.000001$ record $M_{\infty,n}$ then compute

$$P_\infty = \frac{P_1}{\xi_n} \tag{3}$$

and

$$P_{\infty,t} = P_\infty(1 + 0.2M_{\infty,n}^2)^{7/2} \tag{4}$$

Compute Θ from

$$\Theta = \sin^{-1}\sqrt{\frac{6\xi_n + 1}{7M_{\infty,n}^2}} \tag{5}$$

and δ - α from

$$\delta - \alpha = \sin^{-1}\sqrt{\frac{6\xi_n + 1}{7M_{\infty,n}^2}} - \sin^{-1}\sqrt{\frac{\xi_n + 6}{7M_1^2\xi_1}} \tag{6}$$

and α from

$$\alpha = \delta - (\delta - \alpha) \tag{7}$$

with δ = 0.1396 radians and (δ - α) from equation (6).

**THE CALCULATION FOR $M_1$ FOLLOWS**:

Formula for first guess of $M_1$ (= $M_{1,1}$). From normal shock relations

$$\frac{P_{2,t}}{P_1} = \left(\frac{6}{7M_1^2 - 1}\right)^{5/2}\left(\frac{6M_1^2}{5}\right)^{7/2}$$

with

$$7M_1^2 \gg 1$$

$$7M_1^2 - 1 \to 7M_1^2$$

then

$$2_t \frac{P_{2,t}}{P_1} \sim \left(\frac{36}{35}\right)^{5/2} \frac{6}{5} M_1^2$$

and

$$M_1^2 \approx \frac{5}{6}\left(\frac{36}{35}\right)^{5/2} \frac{P_{2,t}}{P_1}$$

The first guess for $M_1$, i.e., $M_{1,1}$, is

$$M_{1,1} = 0.8813 \left(\frac{P_{1_t}}{P_1}\right)_{measured}^{1/2}$$

Substitute the first guess for $M_1 = M_{1,1}$ into

$$\frac{P_{2,t}}{P_1} = \frac{166.926 M_{1,n}^7}{\left(7M_{1,n}^2 - 1\right)^{5/2}} \tag{1a}$$

Check to see if

$$\frac{\left|\left(\frac{P_{2,t}}{P_1}\right)_{measured} - \left(\frac{P_{2,t}}{P_1}\right)_n\right|}{\left(\frac{P_{2,t}}{P_1}\right)_{measured}} > or < 0.0001$$

If

$$\frac{\left|\left(\frac{P_{2,t}}{P_1}\right)_{measured} - \left(\frac{P_{2,t}}{P_1}\right)_n\right|}{\left(\frac{P_{2,t}}{P_1}\right)_{measured}} < 0.0001$$

put $M_{1,n} = M_1$ and proceed with the calculation of

$$\frac{P_{1,t}}{P_1} = \left(\frac{M_1^2 + 5}{5}\right)^{\frac{7}{2}}$$

which is step 3 in the data reduction procedure.

If

$$\frac{\left|\left(\frac{P_{2,t}}{P_1}\right)_{measured} - \left(\frac{P_{2,t}}{P_1}\right)_n\right|}{\left(\frac{P_{2,t}}{P_1}\right)_{measured}} > 0.0001$$

substitute $\left(\frac{P_{2,t}}{p_1}\right)_{measured}$ from $M_{1,n}$ into

$$M_{1,n+1} = M_{1,n}\left\{1 + \frac{\left(\frac{P_{2,t}}{P_1}\right)_{measured} - \left(\frac{P_{2,t}}{P_1}\right)_n}{\left(\frac{P_{2,t}}{P_1}\right)_{measured}}\right\}$$

to get $M_{1,n+1}$ which, in turn, is substituted into equation (1a) and the process is repeated.

**Symbols**

| | |
|---|---|
| $M_1$ | Mach number behind shock from wedge leading edge |
| $M_\infty$ | Mach number ahead of probe |
| $P_\infty$ | static pressure just ahead of probe |
| $P_1$ | static pressure behind shock from wedge leading edge |
| $P_{o,1}$ | total pressure behind normal shock wave in flow ahead of wedge |
| $P_{2,t}$ | total pressure behind normal shock wave in flow behind wedge leading edge shock |
| $\alpha$ | angle of attack of model or angle of flow to wedge probe |
| $\delta$ | wedge semi-angle |
| $\theta$ | angle that shock from wedge leading edge makes with wedge |
| $\xi$ | $= P_1 / P_\infty$ |

**Subscripts**

| | |
|---|---|
| E | quantity from experiment |
| f | first iteration |
| n | number of iterations |
| t | total or stagnation |

# Appendix B

## Procedure for Calculating the Free-Stream Variables from the Measured Quantities for the Conical Probe

The measured quantities are $H_T$, $P_{c,lo}$, $P_{c,u}$, $P_{c,l}$, $P_{c,r}$, $T_{meas}$ and $P_i$. The basic equation for Mach number and flow-angle equations are:

$$M_{\infty,n} = 0.2637 + 0.5397\left(\frac{H_T}{P_{c,av}}\right) - 0.0158\left(\frac{H_T}{P_{c,av}}\right)^2 + \frac{i_n}{1000}\left[0.673 - 0.657\left(\frac{H_T}{P_{c,av}}\right) + 0.127\left(\frac{H_T}{P_{c,av}}\right)^2\right] \tag{1}$$

$$i_{n+1}^2 = \alpha_{n+1}^2 + \beta_{n+1}^2 \tag{2}$$

$$\alpha_{n+1} = \frac{P_{c,lo} - P_{c,u}}{H_T}\left(59.5 - \frac{14.7}{M_{\infty,n}} + \frac{39.4}{M_{\infty,n}^2}\right) \tag{3}$$

$$\beta_{n+1} = \frac{P_{c,l} - P_{c,r}}{H_T}\left(59.5 - \frac{14.7}{M_{\infty,n}} + \frac{39.4}{M_{\infty,n}^2}\right) \tag{4}$$

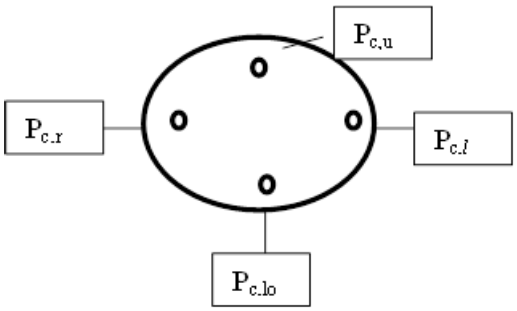


$$P_{c,av} = \frac{P_{c,u} + P_{c,l} + P_{c,lo} + P_{c,r}}{4} \tag{5}$$

Calculation procedure:

With the measured quantities $H_T$ and $P_{c,av}$, see equation (5), and with $i_n$ set equal to zero, i.e., $i_n = i_1 = 0$, calculate

$$M_{\infty,n} = M_{\infty,1}$$

from equation (1).

Then with $M_{\infty,1}$ and measured pressure calculate $\alpha_{n+1} = \alpha_2$ and $\beta_{n+1} = \beta_2$ and

$$i_{n+1}^2 = i_2^2 = \alpha_2^2 + \beta_2^2$$

from equations (3), (4), and (2).

Then increase index n to 2, i.e., n = 2, in equation (1) and calculate $M_{\infty_2}$ using $i_2$.

With $M_{\infty,2}$ and $M_{\infty,1}$, check to see $M_{\infty,n} - M_{\infty,n-1} = M_{\infty,2} - M_{\infty,1} \leq 0.002$

If not, continue calculation with $M_{\infty_2}$ to obtain $\alpha_3$, $\beta_3$, and $i_3$ from equations (2), (3), and (4), and with an index in equation (1) increased to 3 (i.e. n = 3) and calculate $M_{\infty,3}$. Then check $M_{\infty,n} - M_{\infty,n-1} = M_{\infty,3} - M_{\infty,2} \leq 0.002$, and so on until the test is satisfied.

Once $M_\infty$ is determined, calculate

$$P_{t_\infty} = H_T \left[\frac{7M_\infty^2 - 1}{6}\right]^{5/2} \left[\frac{6M_\infty^2}{M_\infty^2 + 5}\right]^{-7/2} \tag{6}$$

and with $P_{t_\infty}$ from equation (6) calculate

$$P_\infty = P_{t,\infty} (1 + 0.2M_\infty^2)^{-\frac{7}{2}} \tag{7}$$

Also with measured $T_{meas}$, $H_T$, and $P_i$ calculate

$$T_2 = T_{meas} \left(\frac{H_T}{P_i}\right)^{2/7} \tag{8}$$

With

$$T_{t,\infty} = T_2 \tag{9}$$

and $P_{t,\infty}$ from equation (6) the total free-stream density can be determined by

$$\rho_{t,\infty} = \frac{P_{t,\infty}}{RT_{t,\infty}} \tag{10}$$

The free-stream temperature is determined by

$$T_\infty = T_{t,\infty}(1 + 0.2M_\infty^2)^{-1} \tag{11}$$

using $T_{t,\infty}$ from equation (9).

And with $T_\infty$ the free-stream static speed of sound can be determined by

$$a_\infty = \sqrt{1.4RT_\infty} \tag{12}$$

With this quantity and the converged value for $M_\infty$, free-stream velocity is obtained.

$$V_\infty = M_\infty a_\infty \tag{13}$$

Finally, if acceleration is of interest, it can be determined using the time-varying velocity from equation (13).

$$Acceleration = \frac{\Delta V_\infty(t)}{\Delta t}$$

The rate of change of Mach number with time can be calculated in a similar fashion using the Mach number calculated by equation (1).

**Symbols**

| | |
|---|---|
| $M_\infty$ | free-stream Mach number |
| $H_T$ | measured total pressure behind shock at apex cone |
| $P_{c,av}$ | average static pressure |
| $P_{c,lo}$ | static pressure at lower port |
| $P_{c,u}$ | static pressure at upper port |
| $P_{c,l}$ | static pressure at left-hand port |
| $P_{c,r}$ | static pressure at right-hand port |
| $\alpha$ | angle of attack |
| $\beta$ | angle of sideslip |
| i | total flow incidence angle |
| $P_{t,\infty}$ | free-stream total pressure |
| $P_\infty$ | free-stream static pressure |
| $P_i$ | pressure in channel ahead of temperature probe |
| R | gas constant |
| $T_2$ | total temperature inside cone |
| $T_{meas}$ | temperature measured inside cone |
| $T_{t,\infty}$ | total free-stream temperature |
| $T_\infty$ | static free-stream temperature |
| $\rho_{t,\infty}$ | total free-stream density |
| $a_\infty$ | free-stream speed of sound |
| $V_\infty$ | free-stream velocity |

**Subscripts**

| | |
|---|---|
| n | index |
| 1 | first iteration |
| $\infty$ | free stream |

# Appendix C

## Results and Discussion of Non-Temperature-Corrected Wind-Tunnel Data

It was noted in the text that the calibration of the miniature pressure sensors for the wind-tunnel tests was only carried out at room temperature, since it was assumed that the gages were all properly temperature compensated. As also noted in the text, this was not the case. Since the gages in the flight tests used for the wedge probe were the same as those in the wind tunnel, the calibrations of these gages performed at the Dryden Flight Research Center over a range of temperatures from -50 °F to 140 °F were valid for the wind-tunnel data reductions. Thus, the wind-tunnel data could be re-calculated for the appropriate temperature and are presented in the main body of the report. In this Appendix, the wind-tunnel data, calculated using room temperature calibrations, are presented. It is thought that the relative magnitude of the calculated data using room-temperature calibration is qualitatively relevant and of interest.

### Wind-Tunnel Flow Angle Measurements

Measurements by the wedge and conical probes were made at three nominal Mach numbers, 1.6, 1.8, and 2.0, and the angles of attack were varied from -4° to +8° angle of attack. Data for these three Mach numbers are plotted in figure C1. Figure C1a, for a nominal Mach number of 1.6, shows that the measurements of both probes are almost linear with angle of attack. The wedge probe measurements agree quite well with the wind-tunnel measurements but the conical probe values are higher by ~0.5°

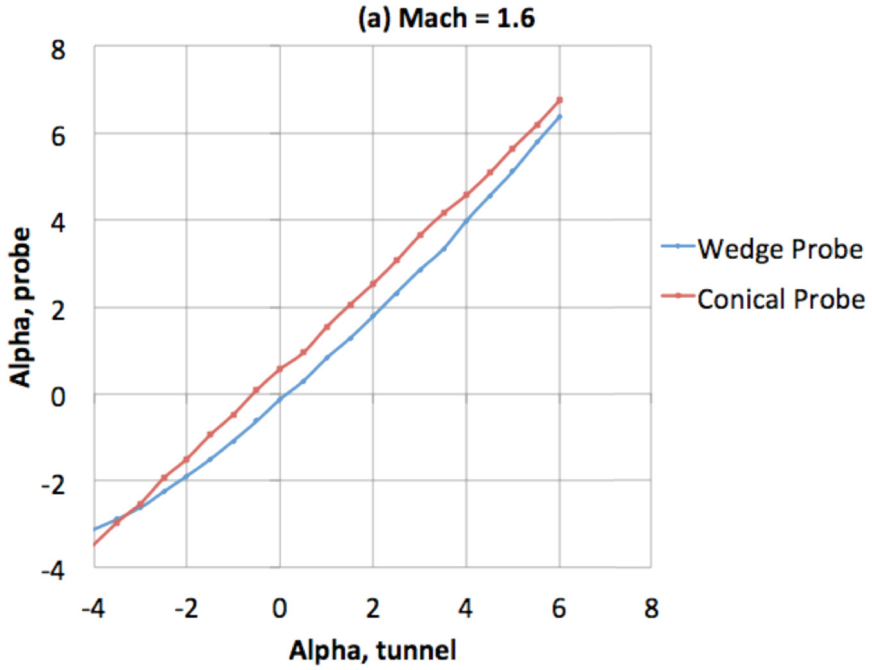


Figure C1. Comparison of probe measured flow angle to wind-tunnel angle-of-attack setting for three Mach numbers.

For a nominal Mach number of 1.8 (fig. C1b) the wedge probe and the wind-tunnel angle-of-attack data agree but the conical probe measured angle of attack is consistently about 0.8° higher. Both sets of data are linear with angle of attack.

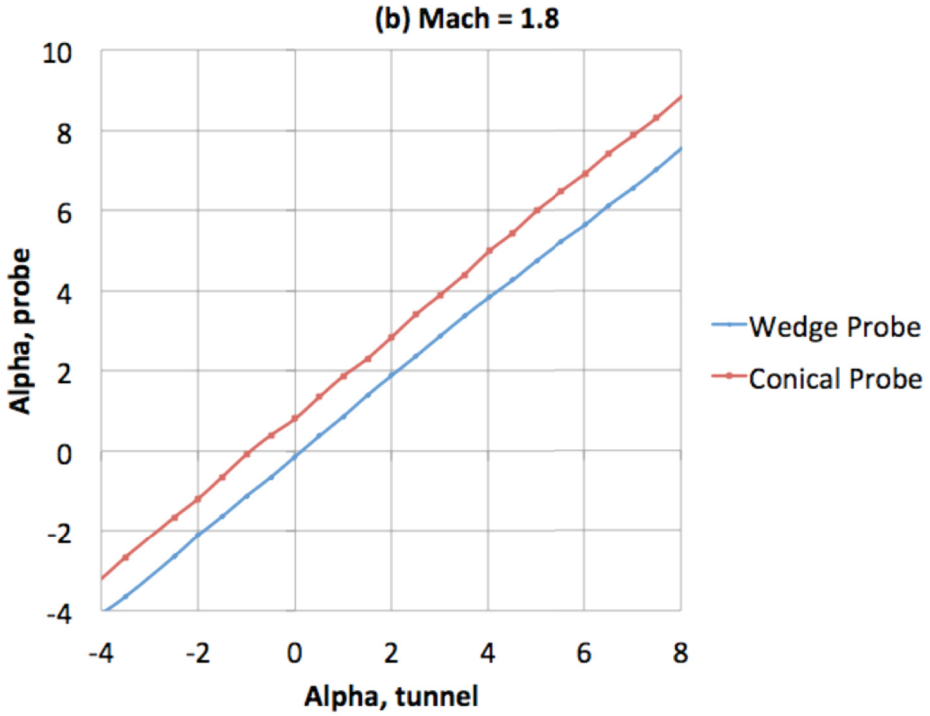


Figure C1. Continued.

For the nominal Mach 2.0 plot, figure C1c, neither set of data agrees with the wind-tunnel angle-of-attack measurement, although the wedge probe data are close. However, wind-tunnel flow-quality data at a Mach number of 2.0 indicate that there is clearly a flow angle at both the wedge and conical probes of ~ 0.5°, which then moves both the wedge and conical probe data further from the wind-tunnel data. Also, it appears that the conical probe is misaligned about 0.8° with the wedge probe, thus, if the cone data are translated down ~ 0.8° in figures C1, then the flow-angle data would make more sense.

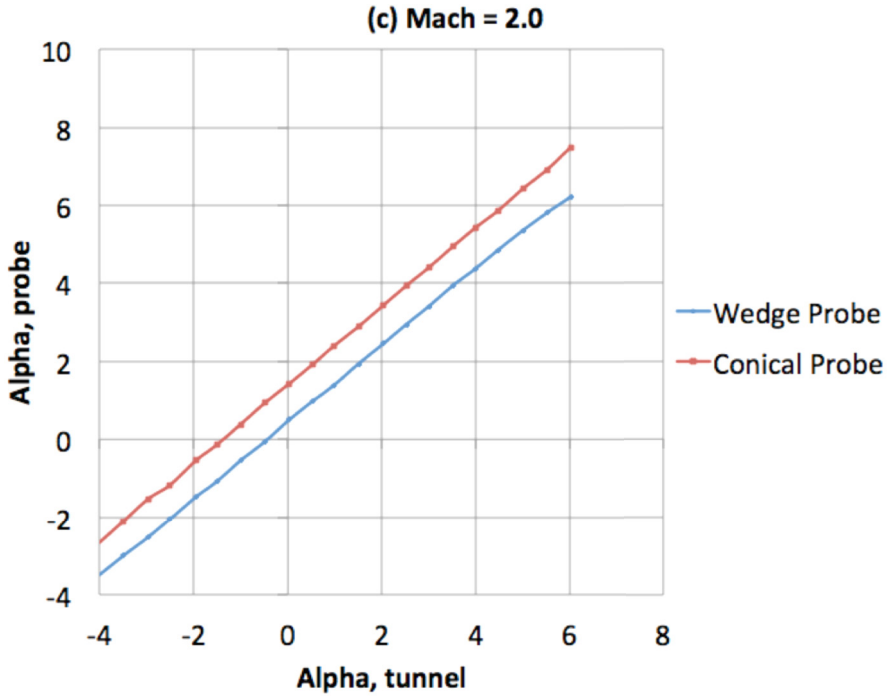


Figure C1. Concluded.

## Wind-Tunnel Static-Pressure Measurements

Since the pressure data are the quantities used in boom propagation codes, they are of particular interest. Figure C2 shows the static pressure data for the three nominal Mach numbers for the wedge and conical probes as well as the 2° cone.

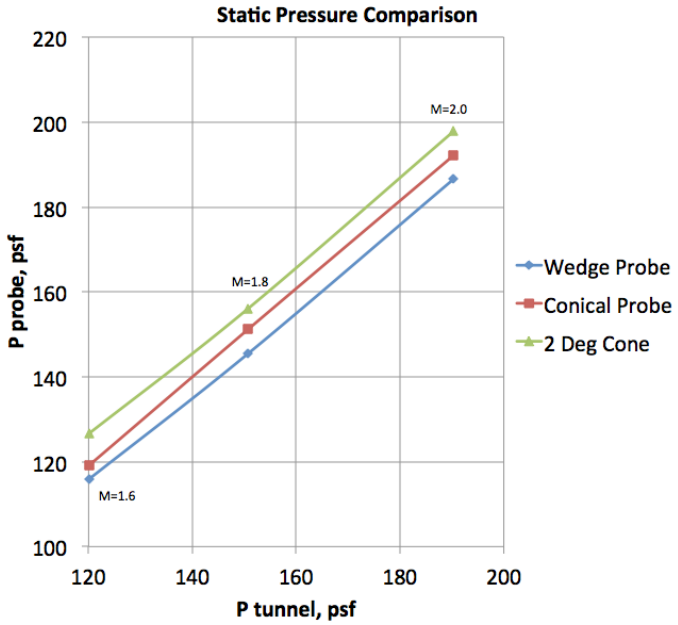


Figure C2. Comparison of probe-measured pressure to wind-tunnel values for three Mach numbers.

The data for the conical probe are about 5 psf higher than the wedge probe, which is not bad considering that they are located 10 inches apart in a non-uniform free stream. Data for the 2° cone are about 3 to 3.5 percent higher than those for the conical probe. The fact that the 2° cone reads high could be because no account was made of the shock off its apex as for the other probes.

## Wind-Tunnel Static Mach Number Measurements

Mach numbers determined by the wedge and conical probes, as well as for the 2° cone, are plotted in figure C3 as a function of the wind-tunnel Mach number. The wedge and conical probe values are about 0.025 Mach different, with the wedge probe being the highest. The 2° cone values are the lowest, which is consistent with the fact that no account is made of the effect of the shock off its apex. All values are within a percent or two of those determined by the wind-tunnel system.

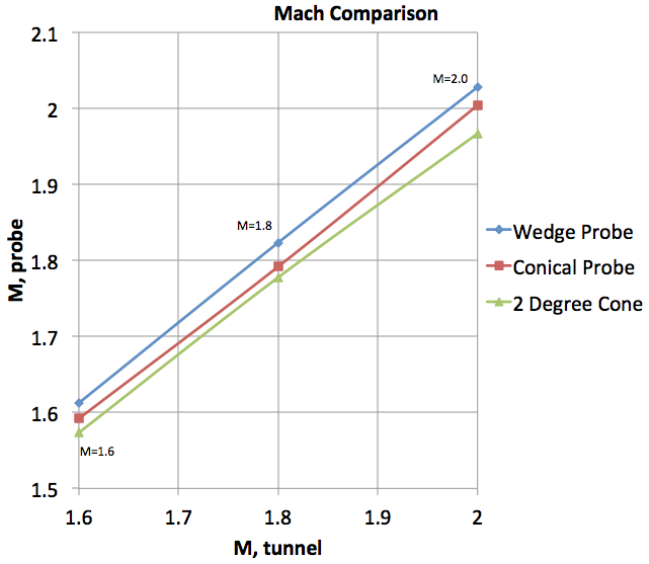


Figure C3. Comparison of probe-measured Mach number to wind-tunnel setting.

Note that the wedge and conical probes use the measured total pressure at the wedge probe gage location, while the Mach number of the wind-tunnel system, and the calculation of that for the 2° cone, use a value determined upstream.

## Wind-Tunnel Transient Pressures due to Shock Generator

Pressure distributions created by moving the probes longitudinally through the flow field created by the shock generator (wall disturbance bump), over a distance of about 14 inches are discussed in this sub-section. For the wedge probe the leading-edge shock from the generator is encountered at an x of ~ 3.0 inches (see fig. C4) and it has a strength of 0.3 psi. It appears to have been resolved in 0.3 inches of the travel. The bow shock is followed by a steady pressure recovery. There is a slight increase in pressures starting around x = 5.5 inches which, is probably due to the secondary shock generator.

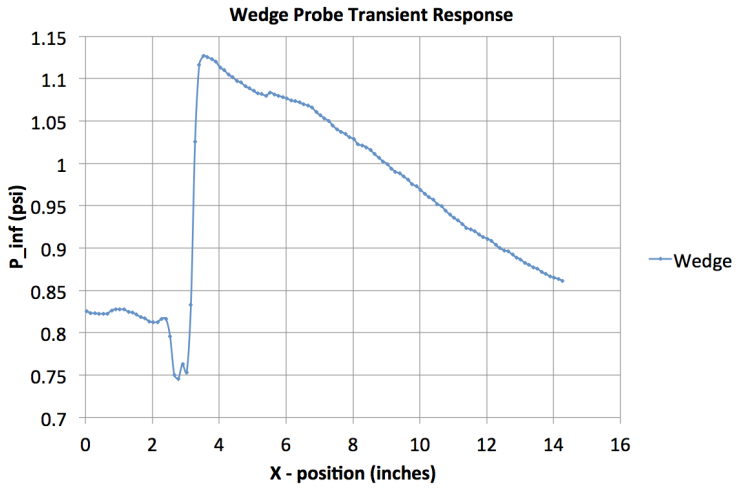


Figure C4. Response of wedge probe to disturbance bump shock.

The pressure distribution created by the shock generator (wall disturbance bump), as measured by the conical probe, is shown in figure C5 compared to that of the wedge probe. Since the apex of the cone of the conical probe is ~1 inch ahead of leading edge of the wedge, the shock from the generator is felt ~1 inch ahead of that felt by the wedge probe. Also, the shock is more smeared than for the wedge probe since the static-pressure measurement on the cone is ~0.75 inches downstream of the apex where the total pressure is measured. It may be recalled that total pressure measured by the wedge probe orifice is used for the conical probe. It appears that the shock jump is essentially the same once the transients, due to the wall boundary layer and the separation of the pressure ports, are taken into account, as is the pressure recovery following the shock. It should be remembered that in flight, which the conical probe is designed for, where the signature lengths are greater than the length of the aircraft, the smearing seen in these tests will not be a factor.

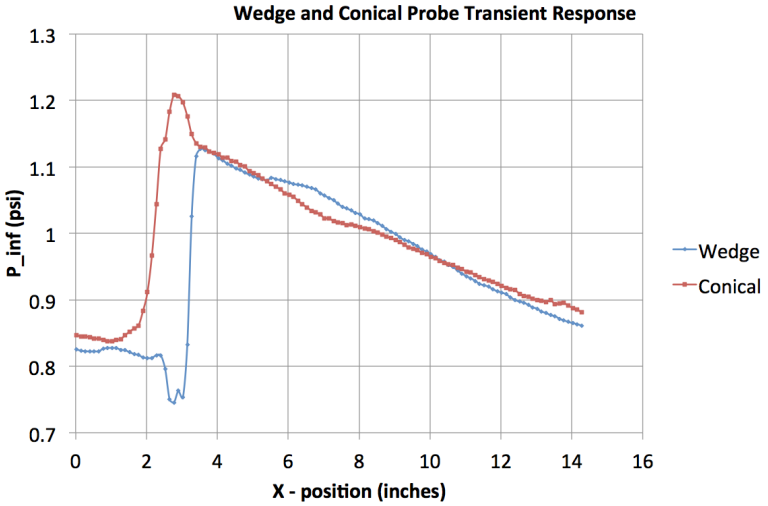


Figure C5. Response of wedge probe and conical probe to disturbance bump shock.

Figure C6 shows the pressure distribution, due to the shock generator (wall disturbance bump), measured by the 2° cone compared to the wedge probe measurement. Its pressure orifices are located about a half-inch ahead of the leading edge of the wedge probe and, thus, it senses the shock

jump ahead of the wedge by this amount. The gradual pressure recovery downstream of the shock has about the same gradient as the wedge probe but the values are consistently 2 to 3 percent lower than the wedge-probe values. It is not clear if this is a result of the variable flow field or the use of the wind-tunnel-system total-pressure measurement. However, the pressure recovery beyond an x of 10 inches has a smaller gradient than that of the wedge probe. This is a different phenomenon from the smearing of the abrupt shock jump that is seen in this figure, as well as that shown in figure 7 of the text.

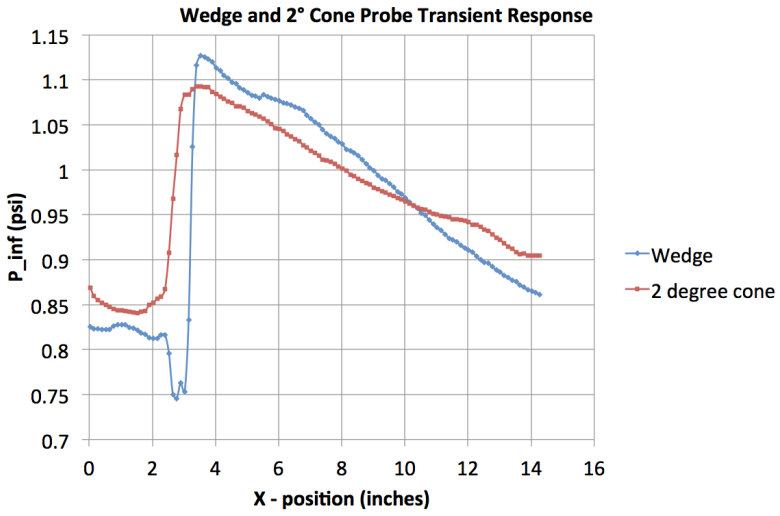


Figure C6. Response of wedge probe and 2° cone probe to disturbance bump shock.

## Wind-Tunnel Transient Measurements of Mach Number

The variation of Mach number with distance was measured by the wedge and conical probes using the wedge-measured total pressure. The 2° cone's static pressure was used with the wind-tunnel-system-measured total pressure for this calculation.

Figure C7 shows the variation with x of the Mach number for the wedge probe. There is a slight increase in Mach number ahead of the shock jump due to the fact that all three pressure sensors are not exposed to the shock at the same time or an artifact of the processing of the shock by the wall boundary layer. Behind the shock the Mach number drops abruptly to 1.8. It is followed by a Mach recovery that lasts out to the end of the measurements. Note that there is an inflection beyond at x of 5 that is thought to be due to the secondary shock generator.

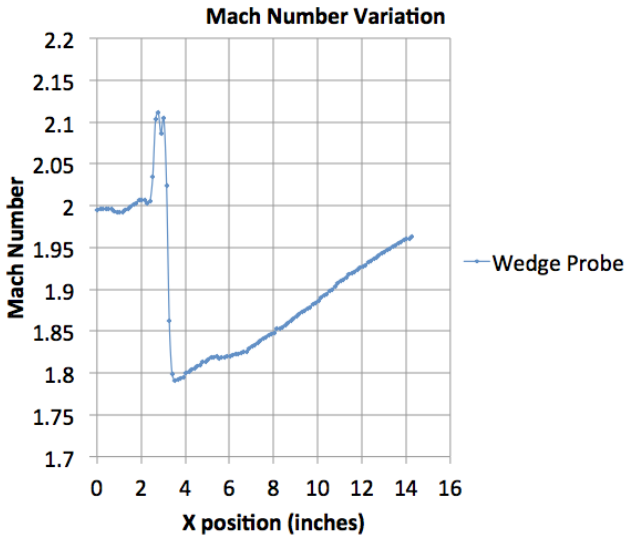


Figure C7. Variation of Mach number across wall disturbance shock as measured by wedge probe for wind tunnel, nominal Mach number of 2.0.

The x variation of the conical probe's Mach measurements is plotted in figure C8 along with that of the wedge probe. For these calculations the free-stream total pressure measured by the wedge probe was used (as noted earlier) as it was for the pressure and flow-angle measurements. Since this sensor is ~ 1 inch behind the apex of the cone, its measured values were translated forward by this amount to use in the conical-probe calculations. Due to the different geometry of the cone and the location of its sensors there is more reduction of the gradient beyond an x of 8 inches as was the case for the pressure. Note that the pressures are used in the calculation of the Mach number. It is also clear from other measurements and the wind-tunnel survey plots of figure 19 that there are variations in total pressure (lateral and longitudinal) in the test region of these probes. One evidence of this is the difference in Mach number at x = 0.

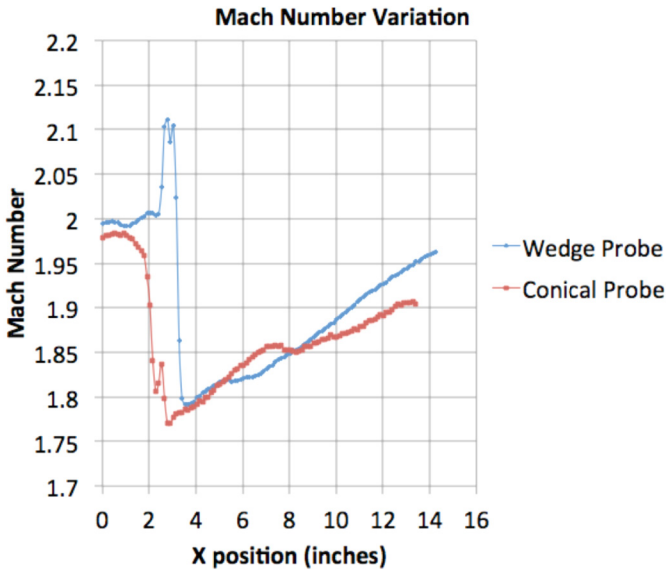


Figure C8. Variation of Mach number across wall disturbance shock as measured by wedge probe and conical probe for wind tunnel, nominal Mach number of 2.0.

While the 2° cone is not normally used for Mach number measurements (and it would not be useful in flight) it is possible to calculate Mach number using the 2°-cone-measured static pressure and the wind-tunnel-measured total pressure (as noted earlier). The results are presented in figure C9 along with the wedge-probe results. As with the other probes, the shock jump is smeared. It produced the highest Mach numbers downstream of the shock jump and the gradient in Mach number beyond an x of 6.0 is smaller than that of the wedge probe.

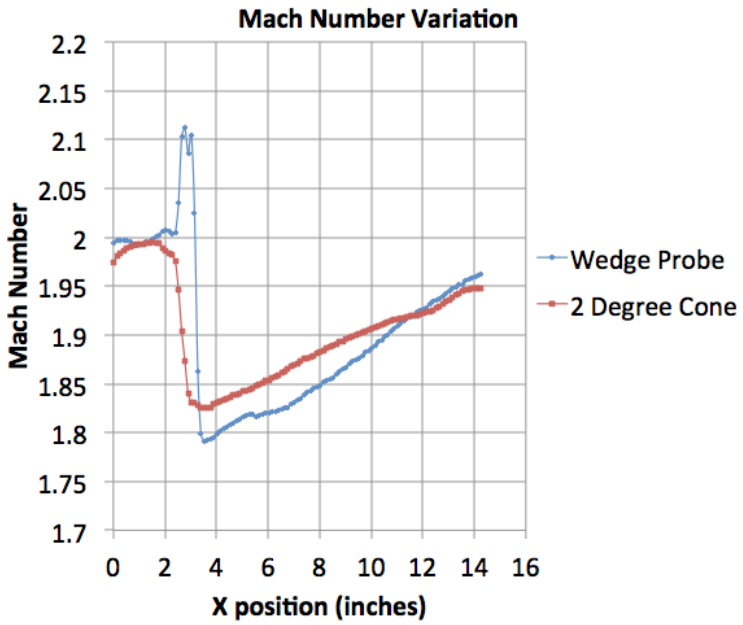


Figure C9. Variation of Mach number across wall disturbance shock as measured by wedge probe and the 2° cone for wind tunnel, nominal Mach number of 2.0.